Cell Research

www.nature.com/cr
www.cell-research.com

ARTICLE

Oncogenic AURKA-enhanced N^6-methyladenosine modification increases *DROSHA* mRNA stability to transactivate *STC1* in breast cancer stem-like cells

Fei Peng[1,2], Jie Xu[1], Bai Cui[1], Qilan Liang[1], Sai Zeng[1], Bin He[2], Hong Zou[1], Manman Li[1], Huan Zhao[1], Yuting Meng[1], Jin Chen[3], Bing Liu[1], Shasha Lv[1], Peng Chu[1,4], Fan An[1], Zifeng Wang[2], Junxiu Huang[1], Yajing Zhan[1], Yuwei Liao[1], Jinxin Lu[1], Lingzhi Xu[5], Jin Zhang[6], Zhaolin Sun[4], Zhiguang Li[1], Fangjun Wang[3], Eric W.-F. Lam[7] and Quentin Liu[1,2]

RNase III DROSHA is upregulated in multiple cancers and contributes to tumor progression by hitherto unclear mechanisms. Here, we demonstrate that DROSHA interacts with β-Catenin to transactivate *STC1* in an RNA cleavage-independent manner, contributing to breast cancer stem-like cell (BCSC) properties. *DROSHA* mRNA stability is enhanced by N^6-methyladenosine (m^6A) modification which is activated by AURKA in BCSCs. AURKA stabilizes METTL14 by inhibiting its ubiquitylation and degradation to promote *DROSHA* mRNA methylation. Moreover, binding of AURKA to *DROSHA* transcript further strengthens the binding of the m^6A reader IGF2BP2 to stabilize m^6A-modified *DROSHA*. In addition, wild-type *DROSHA*, but not an m^6A methylation-deficient mutant, enhances BCSC stemness maintenance, while inhibition of *DROSHA* m^6A modification attenuates BCSC traits. Our study unveils the AURKA-induced oncogenic m^6A modification as a key regulator of *DROSHA* in breast cancer and identifies a novel DROSHA transcriptional function in promoting the BCSC phenotype.

Cell Research (2020) 0:1–17; https://doi.org/10.1038/s41422-020-00397-2

INTRODUCTION

DROSHA processes primary miRNAs into precursor miRNAs. Accumulated evidence further reveals that DROSHA directly regulates diverse RNA metabolism across the transcriptome, including post-transcriptional control of RNA stability,[1] alternative splicing,[2] 3′-end processing[3] and transcriptional termination.[4] Pathologically, DROSHA is aberrantly expressed in multiple cancer types,[5] and contributrun 0tes to cancer progression through its miRNA processing and RNA cleavage functions.[6,7] A recent study reports that DROSHA specifically binds proximal promoter regions to induce gene transcription through complexing with CBP80 and RNA Polymerase II.[8] Yet, how this transcriptional role of DROSHA promotes tumor development and the underlying mechanisms involved are much less well understood. In addition, previous studies have revealed that *DROSHA* is transcriptionally regulated by key oncogenes in cancers. For instance, c-Myc directly binds to the E-box of *DROSHA* promoter to activate its transcription in B lymphoma cells and lung cancer cells.[9] However, the regulation of *DROSHA* mRNA stability during tumor development remains unknown.

m^6A is a highly prevalent modification in mRNA[10] and is recognized by m^6A-binding proteins (readers) that determines mRNA fate, through modulating their splicing, translation, or stability.[11] m^6A modification is catalyzed by a core METTL3-METTL14-WTAP m^6A methyltransferase complex (writer) and removed by two key eraser enzymes (FTO and ALKBH5), and these factors are essential for cancer initiation and progression.[12] For example, ALKBH5 demethylates *FOXM1* nascent transcripts and enhances FOXM1 expression via lncRNA *FOXM1-AS* to promote tumorigenicity of glioblastoma stem-like cells.[13] METTL14, negatively regulated by transcription factor SPI1, elevates the expression of oncogenes *MYB* and *MYC* via m^6A modification to stimulate acute myeloid leukemia (AML) development and leukemia stem cell (LSC) self-renewal.[14] Moreover, the m^6A reader YTHDF2 represses mRNA stability of methylated tumor suppressor *SOCS2* to promote tumor growth and lung metastasis in hepatocellular carcinoma.[15] In contrast, newly identified m^6A reader proteins (IGF2BP1-3) also play oncogenic roles in cancers by stabilizing methylated mRNA of oncogenic targets (especially, *MYC*).[16] Thus, whether m^6A modification regulates *DROSHA* mRNA stability to promote tumorigenicity is worth investigating.

The Aurora kinase A (AURKA) oncogene is overexpressed in a variety of tumors and plays multiple roles in cancer development.[17] Our recent study also demonstrates that AURKA displays a

[1]Institute of Cancer Stem Cell, Dalian Medical University, Dalian, Liaoning 116044, China; [2]State Key Laboratory of Oncology in South China, Cancer Center, Sun Yat-sen University, Guangzhou, Guangdong 510060, China; [3]Key Laboratory of Separation Sciences for Analytical Chemistry, National Chromatographic R&A Center, Dalian Institute of Chemical Physics, Chinese Academy of Sciences (CAS), Dalian, Liaoning 116023, China; [4]Institute of Integrative Medicine, Dalian Medical University, Dalian, Liaoning 116044, China; [5]Department of Oncology, the Second Affiliated Hospital, Dalian Medical University, Dalian, Liaoning 116023, China; [6]The 3rd Department of Breast Cancer, China Tianjin Breast Cancer Prevention, Treatment and Research Center, Tianjin Medical University Cancer Institute and Hospital, National Clinical Research Center of Cancer, Tianjin, Tianjin 300060, China and [7]Department of Surgery and Cancer, Imperial College London, London, W12 0NN, UK
Correspondence: Jie Xu (xujie@dmu.edu.cn) or Quentin Liu (liuq9@mail.sysu.edu.cn)
These authors contributed equally: Fei Peng, Jie Xu, Bai Cui, Qilan Liang, Sai Zeng, Bin He

Received: 16 February 2020 Accepted: 5 August 2020
Published online: 28 August 2020

nuclear kinase-independent function in transactivating the *MYC* promoter in cooperation with hnRNP K, contributing to breast cancer stem cell traits.[18] Here, our data show that DROSHA interacting with β-Catenin transactivates the stemness gene *STC1* in a non-canonical fashion to promote BCSC properties. Moreover, *DROSHA* mRNA stability is enhanced by m^{6}A modification, which is in turn mediated by the AURKA-METTL14 axis and stabilized by AURKA-IGF2BP2 complex. Depletion of *DROSHA* m^{6}A modification significantly suppresses BCSC phenotype. Altogether, these findings reveal the AURKA-mediated m^{6}A modification as a key regulator of DROSHA expression, and define a transactivating role of DROSHA in BCSC maintenance.

RESULTS

A non-canonical function of DROSHA in promoting *STC1* transcription

As cancer stem-like cells contribute to tumorigenesis,[19] we firstly examined the role of DROSHA in BCSC maintenance. A significant upregulation of both the *DROSHA* mRNA and protein levels, which

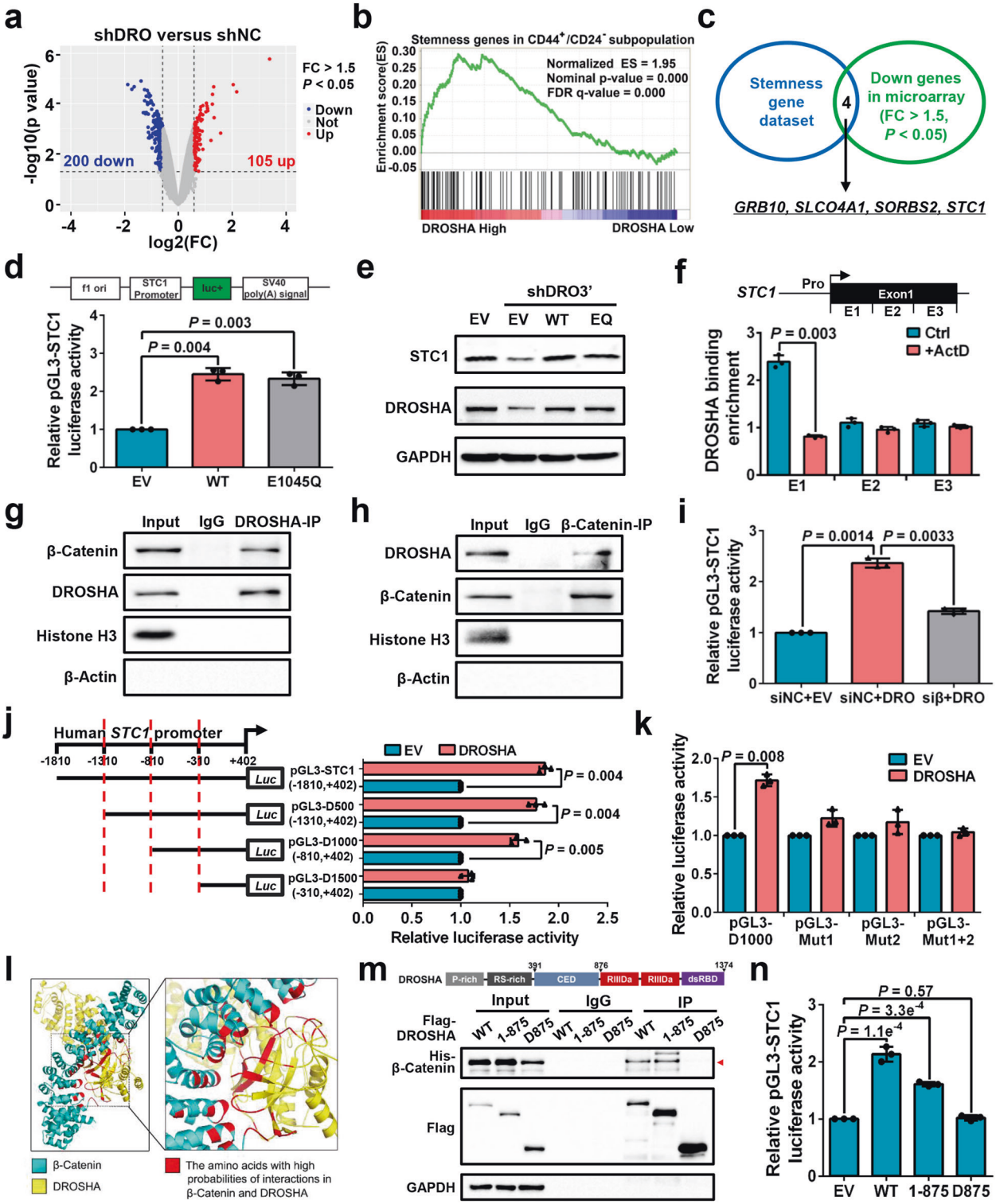

Fig. 1 A non-canonical function of DROSHA in promoting *STC1* transcription. a Volcano plots displaying DEGs in microarray data comparing shDROSHA with shNC MDA-MB-231 cells. The numbers of significantly variant genes (FC > 1.5, $P < 0.05$) were shown. Vertical dashed lines indicate cut-off of FC (1.5), whereas the horizontal dashed lines indicate cut-off of *P* value (0.05). FC, fold change. **b** Upregulated DEGs in shNC group of microarray data were subjected to GSEA using the gene expression signature that was upregulated in the $CD44^+/CD24^-$ signature acquired from a public database (GSE7513). **c** Overlapping stemness gene dataset and downregulated genes in shDROSHA cells from microarray data (FC > 1.5, $P < 0.05$), common genes were listed. **d** Relative luciferase activity of pGL3-STC1 in HEK293T cells with forced expression of WT and E1045Q DROSHA. **e** Western blotting showing STC1 and DROSHA expression in MDA-MB-231 cells with endogenous DROSHA knockdown and forced expression of WT and E1045Q DROSHA. **f** ChIP was performed to quantify the binding of DROSHA to *STC1* in MDA-MB-231 cells with or without 5 μg/mL actinomycin D (ActD). **g**, **h** Co-IP assay to detect the interaction between DROSHA and β-Catenin in the nuclear extraction of MDA-MB-231 cells. Histone H3 as nuclear internal control and β-Actin as cytoplasmic internal control. **i** Relative luciferase activity of pGL3-STC1 in HEK293T cells with knockdown of β-Catenin and forced expression of DROSHA. siβ, siRNA against β-Catenin. **j**, **k** Relative luciferase activity of *STC1* truncated promoters (**j**) and mutant promoters (**k**) in HEK293T cells with overexpression of DROSHA. **l** The simulated interaction diagram of β-Catenin and DROSHA. **m** Ability of the indicated Flag-labeled DROSHA derivatives to co-immunoprecipitate His-tagged β-Catenin defined by immunoblotting in HEK293T cells. **n** Relative luciferase activity of pGL3-STC1 in HEK293T cells with overexpression of the indicated DROSHA derivatives. Data are shown as means ± SD. *P* values were calculated with two-tailed unpaired Student's *t*-test and $P < 0.05$ is considered statistically significant.

were associated with enrichment of stemness factors including *MYC*, *POU5F1*, and *NANOG* (Supplementary information, Fig. S1a, b), was determined in BCSC-enriched spheroids. In breast cancer SK-BR-3 cells with overexpression of wild-type (WT) DROSHA, the proportion of $ALDH^+$ cells were increased (Supplementary information, Fig. S1c, d). Meanwhile, forced expression of DROSHA significantly promoted sphere formation ability in replating sphere formation (Supplementary information, Fig. S1e, f) and extreme limiting dilution assays (Supplementary information, Fig. S1g). In contrast, depletion of DROSHA dramatically inhibited sphere formation abilities (Supplementary information, Fig. S1h–j). Moreover, silencing of DROSHA suppressed tumor growth and tumorigenesis in primary tumor xenograft and secondary limited dilution xenograft assays (Supplementary information, Fig. S1k–m). Clinically, high DROSHA expression predicted an inferior overall survival in breast cancer patients ($n = 1076$), suggesting a significantly unfavorable prognosis and shorter patient lifespan (Supplementary information, Fig. S1n).

Next, we analyzed the differentially expressed genes (DEGs) in microarray data, comparing DROSHA-knockdown with control MDA-MB-231 cells. Two hundred genes were downregulated among the DEGs upon DROSHA knockdown (Fig. 1a). We then performed gene set enrichment analysis (GSEA) and found that the upregulated genes of DROSHA High groups in microarray data are also enriched in the $CD44^+/CD24^-$ BCSC subpopulations (Fig. 1b), indicating that besides its role in RNA cleavage, DROSHA transcriptional activity also contributes to BCSC stemness. We thus overlapped those downregulated genes from DROSHA-knockdown microarray data with the stemness genes.[20,21] The overlapped genes from these two groups include *GRB10*, *SLCO4A1*, *SORBS2*, and *STC1* (Fig. 1c). To validate these candidates, reverse transcription-quantitative polymerase chain reaction (RT-qPCR) was performed and showed *STC1*, *GRB10*, and *SLCO4A1* mRNA levels were downregulated and upregulated, respectively, in the DROSHA-deficient and DROSHA-overexpressing cells (Supplementary information, Fig. S2a, b). Ablation of DROSHA also decreased the protein expression of STC1, GRB10 and SLCO4A1 (Supplementary information, Fig. S2c, d). Both *STC1* and *GRB10* mRNA levels were enriched in sphere cells compared with non-spheroid cells (Supplementary information, Fig. S2e). Specifically, depletion of STC1, but not GRB10, SLCO4A1 or SORBS2, blocked DROSHA-deficiency-mediated $ALDH^+$ subpopulation reduction in MDA-MB-231 cells (Supplementary information, Fig. S2f, g), indicating that STC1 might be critical for DROSHA-regulated BCSCs. High expression of STC1 denoted a poor prognosis for breast cancer patients (Supplementary information, Fig. S2h). To further confirm that DROSHA transactivates *STC1*, forced expression of WT or cleavage function mutation (E1045Q) DROSHA[22] enhanced luciferase activity of the *STC1* promoter reporter (Fig. 1d). Overexpression of WT or E1045Q DROSHA also rescued the STC1 expression in endogenous DROSHA-knockdown cells (Fig. 1e). As DROSHA can bind to proximal promoter regions of human protein-coding genes in a transcription-dependent manner,[8] we also found that DROSHA can bind to the *STC1* Exon 1 (E1) dependent on *STC1* transcription by chromatin immunoprecipitation (ChIP) assay (Fig. 1f; Supplementary information, Fig. S2i).

We next explored how DROSHA activates *STC1* transcription, sought to identify DROSHA-interacting proteins using mass spectrometry analysis (Supplementary information, Table S2) and searched for the regulatory proteins of *STC1* promoter with the assistance of software JASPAR. Comparing the candidates from the two analyses, a transcriptional factor complex, β-Catenin/TCF4, was identified (Supplementary information, Fig. S2j). Indeed, we confirmed the interaction between DROSHA and β-Catenin in the nucleus (Fig. 1g, h). Silencing of β-Catenin also significantly decreased the pre-mRNA, mRNA and protein levels of STC1 in DROSHA-overexpressing cells (Supplementary information, Fig. S2k, l). In addition, depletion of β-Catenin markedly reversed DROSHA-increased luciferase activity of the *STC1* promoter reporter, indicating that β-Catenin is critical for the transcription of *STC1* by DROSHA (Fig. 1i; Supplementary information, Fig. S2m). We next determined the region of *STC1* promoter that is required for DROSHA-activated *STC1* transcription and deletion analysis showed that DROSHA failed to activate *STC1* promoter when the -810 to -310 region of *STC1* promoter was removed (Fig. 1j). As two putative β-Catenin/TCF4 binding motifs are located within the -810 to -310 region of the *STC1* promoter, we constructed three binding motif mutant reporters (Mut1, Mut2 and Mut1 plus Mut2) to perform luciferase assay (Supplementary information, Fig. S2n). Forced expression of DROSHA promoted luciferase activity of the pGL3-D1000 reporter, but had no effects on three mutant reporters (Fig. 1k). Further corroborating the mass spectrometry results, molecular dynamics (MD) simulation revealed 43 combinations of high interaction possibilities between amino acids of DROSHA CED domain (390–875 amino acids) and β-Catenin (Supplementary information, Fig. S2o), with the amino acids responsible for the DROSHA and β-Catenin interaction (red color) displaying spatial proximity (Fig. 1l; Supplementary information, Movie S1). As expected, only N-terminal 875 amino acids of DROSHA (1–875), but not the C-terminus of DROSHA (D875), interacted with His-β-Catenin (Fig. 1m). Importantly, DROSHA D875 failed to transactivate *STC1* (Fig. 1n). Together, these data support a role of the CED domain of DROSHA in the recognition of β-Catenin to promote *STC1* transcription.

DROSHA-STC1 axis promotes breast cancer stem-like cell properties

We next verified the role of DROSHA-STC1 axis in promoting BCSC properties. Overexpression of STC1 elevated $ALDH^+$ subpopulations in DROSHA repressed breast cancer cells (Fig. 2a, b;

Supplementary information, Fig. S3a, b). In addition, forced expression of STC1 restored sphere formation ability in extreme limiting dilution assays (Fig. 2c; Supplementary information, Fig. S3c). Consistently, overexpressing STC1 significantly increased the diameter and number of spheres in DROSHA-deficient cells using replating sphere formation assay (Fig. 2d, e). Next, MDA-MB-231 cells with DROSHA stable knockdown or control cells with overexpression of STC1 were injected into nude mice. Mice inoculated with DROSHA-deficient cells with overexpression of STC1 was shown to form larger tumor masses than the mice injected with DROSHA-deficient cells (Fig. 2f, g). Overexpression of STC1 also rescued DROSHA knockdown-mediated inhibition in tumorigenesis in secondary limited dilution xenograft assays (Fig. 2h; Supplementary information, Fig. S3d). Clinically, mRNA levels of *DROSHA* and *STC1* were highly expressed in 21 breast tumor specimens compared with paired normal breast specimens (Supplementary information, Fig. S3e). As NANOG acts as a BCSC marker,[23] we then performed immunohistochemistry (IHC) staining of DROSHA, STC1 and NANOG, to determine their correlations in breast tumor tissues. DROSHA expression positively correlated with the expression of STC1 and NANOG was shown in breast tumor tissues (Fig. 2i). Hence, our data reveal that DROSHA-STC1 axis has a crucial role in promoting BCSC phenotype.

DROSHA mRNA is stabilized by m^{6}A deposition

We further investigated how *DROSHA* is upregulated in BCSCs. As c-Myc could promote *DROSHA* transcription in B lymphoma cells and lung cancer cells,[9] overexpression of MYC was shown to have no effects on *DROSHA* promoter activity, *DROSHA* mRNA level or DROSHA protein expression in breast cancer cells (Supplementary information, Fig. S4a–c). Moreover, there were no significant differences in *DROSHA* promoter activity and *DROSHA* pre-mRNA level between sphere cells and non-sphere cells (Supplementary information, Fig. S4d, e). In contrast, *DROSHA* mRNA exhibited a longer half-life in sphere cells compared to non-sphere cells (Fig. 3a; Supplementary information, Fig. S4f), suggesting that mRNA stability is responsible for high expression of *DROSHA* in BCSCs. By analyzing the m^{6}A methylated RNA immunoprecipitation sequencing (meRIP-seq) data available for breast cancer cells, we found that abundant m^{6}A peaks were accumulated near *DROSHA* mRNA stop codon including three putative m^{6}A motifs (P1-P3) (Fig. 3b). meRIP-qPCR data further confirmed that m^{6}A methylation had a higher abundance near the *DROSHA* mRNA stop codon in sphere cells compared to non-sphere cells (Fig. 3c). The mRNA expression, protein expression and m^{6}A methylation of DROSHA were also much higher in breast tumor specimens compared to the paired normal breast specimens (Fig. 3d–f).

As 3-deazaneplanocin A (DZNeP) or methionine deprivation has been reported to inhibit RNA methylation,[24,25] dot blot showed that DZNeP treatment or methionine deprivation significantly decreased mRNA m^{6}A methylation in breast cancer cells (Supplementary information, Fig. S4g, h). After treating cells with DZNeP treatment or methionine depletion medium, we found that the m^{6}A modification of *DROSHA* decreased dramatically (Fig. 3g; Supplementary information, Fig. S4i). Both the *DROSHA* mRNA and protein were downregulated in DZNeP-treated or methionine-depleted cells (Fig. 3h, i; Supplementary information, Fig. S4j, k). Furthermore, accelerated *DROSHA* mRNA decay upon DZNeP treatment or methionine depletion was observed in MDA-MB-231 cells (Fig. 3j; Supplementary information, Fig. S4l). DZNeP or methionine depletion also reduced luciferase activity of WT m^{6}A motif *DROSHA* (P1-3), P1 m^{6}A motif mutant *DROSHA* (P1-Mut) and P2 m^{6}A motif mutant *DROSHA* (P2-Mut) reporters, but not that of the P3 m^{6}A motif mutant *DROSHA* (P3-Mut) reporter (Fig. 3k; Supplementary information, Fig. S4m), suggesting that m^{6}A modification of *DROSHA* mRNA at P3 is critical for *DROSHA* mRNA stability. We next confirmed that m^{6}A abundance was decreased in MDA-MB-231 cells after the P3 m^{6}A motif of *DROSHA* mRNA was mutated (Fig. 3l). Indeed, ectopic co-expression studies of WT DROSHA (DRO-WT) and P3 mutant DROSHA (DRO-P3Mut) in endogenous DROSHA-deficient cells showed that the P3 m^{6}A motif mutation remarkably accelerated *DROSHA* mRNA decay (Fig. 3m) and decreased DROSHA protein expression (Supplementary information, Fig. S4n). Moreover, examination of the sequence of *DROSHA* transcript revealed that the P3 m^{6}A motif of *DROSHA* mRNA is highly conserved across species (Fig. 3n). The m^{6}A peaks were found to be enriched near *DROSHA* P3 motif in both human and mouse brain tissues by analyzing published meRIP-seq data (Fig. 3o). Similar results were also detected in hepatocellular carcinoma and lung cancer cells (Supplementary information, Fig. S4o). Thus, these findings demonstrate that BCSC-enriched m^{6}A modification deposited on *DROSHA* transcript plays a crucial role in *DROSHA* mRNA stability in breast cancer cells.

AURKA-stabilized METTL14 maintains *DROSHA* transcript via m^{6}A deposition

We next explored the key oncogenes that control *DROSHA* mRNA expression via m^{6}A modification in BCSCs. To this end, we overlapped the top 100 highly expressed oncogenes from TCGA breast tumors with *DROSHA*-correlated stemness genes (Supplementary information, Table S3), and identified four oncogenes, including *AURKA*, *TK1*, *CCNB2* and *BIRC5* (Fig. 4a). Compared to non-sphere cells, the mRNA levels of *AURKA* and *CCNB2* were significantly enriched in sphere cells (Supplementary information, Fig. S5a). Importantly, depletion of AURKA, but not TK1, CCNB2 or BIRC5, significantly decreased luciferase activity of the *DROSHA* P1-3 reporter, but not that of the P3-Mut reporter (Supplementary information, Fig. S5b, c), indicating that AURKA might act as a key regulator of DROSHA. We further determined whether AURKA regulates *DROSHA* m^{6}A modification and mRNA stability. As expected, overexpression or ablation of AURKA increased or reduced *DROSHA* mRNA m^{6}A methylation, respectively (Fig. 4b; Supplementary information, Fig. S5d), and forced expression of AURKA decelerated *DROSHA* mRNA decay in breast cancer cells (Fig. 4c; Supplementary information, Fig. S5e). Moreover, AURKA enhanced luciferase activity of P1-3, P1-Mut and P2-Mut reporters, but not the P3-Mut reporter (Supplementary information, Fig. S5f).

We next investigated how AURKA upregulates *DROSHA* m^{6}A modification, as our previous study revealed that AURKA acted as a co-transcription factor to transactivate *MYC*.[18] Overexpression and depletion of AURKA increased and decreased the mRNA and protein levels of MYC, respectively (Supplementary information, Fig. S5g–j), while knockdown or overexpression of AURKA had little effects on mRNA levels of the m^{6}A methyltransferases and demethylases (Supplementary information, Fig. S5k, l). Furthermore, we found that the protein expression of core methyltransferase METTL14, but not other methyltransferases, demethylases and readers, was consistently downregulated in AURKA-knockout cells and upregulated in AURKA-overexpressing cells (Fig. 4d; Supplementary information, Fig. S5m). Inhibition of AURKA kinase activity also displayed no effects on METTL14 expression (Supplementary information, Fig. S5n), indicating AURKA regulates METTL14 expression in a kinase-independent manner. After treatment with the protein synthesis inhibitor cycloheximide (CHX), knockout of AURKA shortened the half-life of endogenous METTL14 protein (Fig. 4e), whereas overexpression of AURKA resulted in the prolonged half-life of endogenous METTL14 protein (Supplementary information, Fig. S5o). We next treated cells with the proteasome inhibitor MG132 in the absence of AURKA. MG132 enhanced METTL14 expression, whereas AURKA knockout did not decrease DROSHA level in the presence of MG132 treatment (Fig. 4f), suggesting that AURKA stabilizes METTL14 protein expression through inhibition of the proteasome-dependent degradation pathway. Moreover, we found that overexpression of AURKA reduced METTL14 ubiquitylation (Fig. 4g), whereas knockdown of AURKA increased METTL14

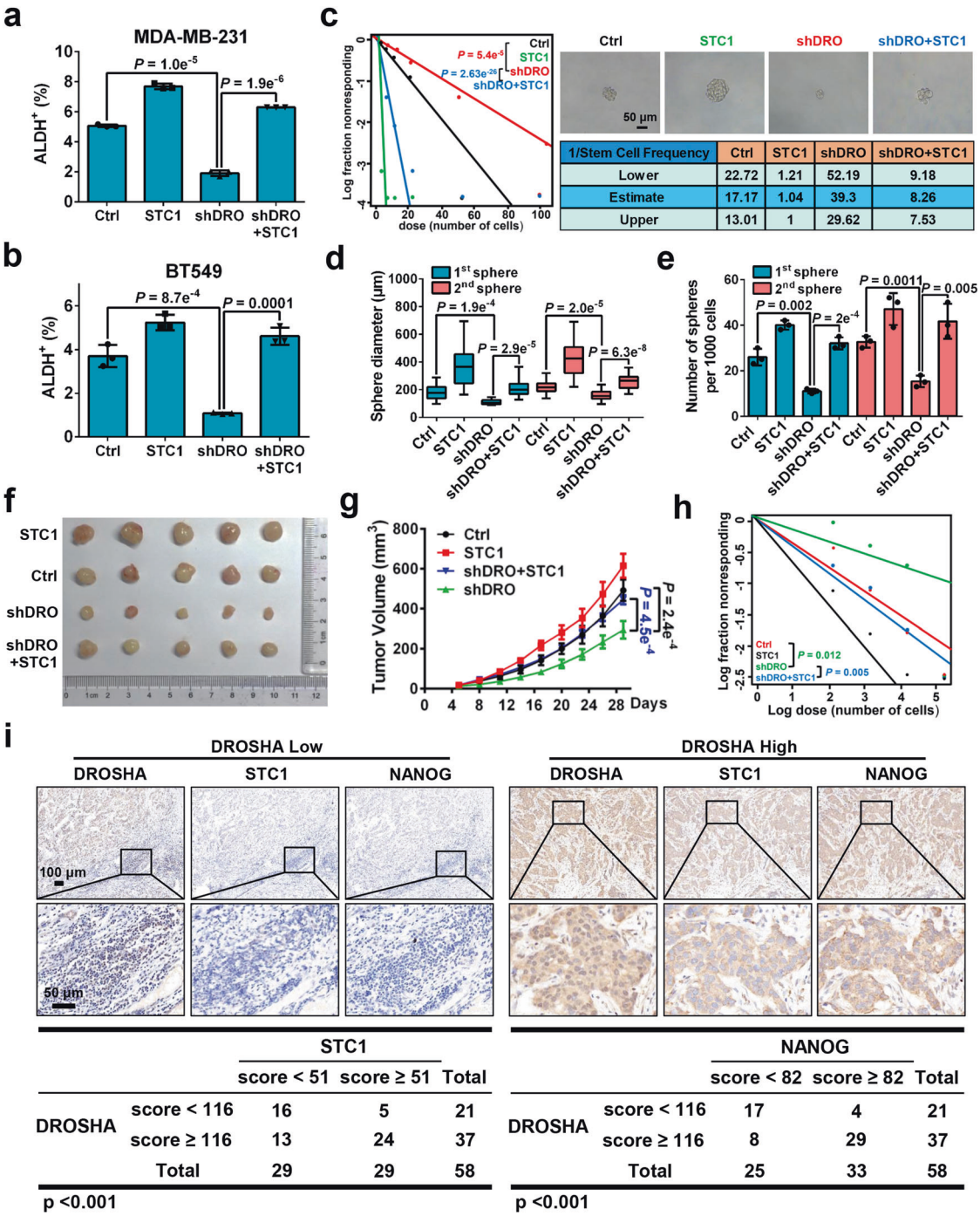

STC1		score < 51	score ≥ 51	Total
DROSHA	score < 116	16	5	21
	score ≥ 116	13	24	37
	Total	29	29	58

p <0.001

NANOG		score < 82	score ≥ 82	Total
DROSHA	score < 116	17	4	21
	score ≥ 116	8	29	37
	Total	25	33	58

p <0.001

Fig. 2 DROSHA-STC1 axis promotes BCSC properties. a, **b** ALDH$^+$ populations were analyzed in MDA-MB-231 (**a**) and BT549 (**b**) cells with DROSHA knockdown and forced expression of STC1. shDRO, shRNA against *DROSHA*. STC1, overexpression of STC1. **c** Left: ELDA was performed in MDA-MB-231 cells with DROSHA knockdown and forced expression of STC1. Top right: The representative sphere images are shown. Scale bars, 50 μm. Bottom right: Stemness frequency illustration of the cells with the upper and lower 95% confidence intervals meaning that the frequency of one stem cell in cancer cells. Spheres were counted from 24 replicate wells. **d**, **e** Replating sphere formation was performed in MDA-MB-231 cells with DROSHA knockdown and forced expression of STC1. The diameter (**d**) and number (**e**) of spheres were quantified. Spheres were counted from three replicate wells. The diameter and number of each experiment represent the total count of three replicate wells. **f**, **g** Immunodeficient mice ($n = 5$, biological replicates) were subcutaneously inoculated with MDA-MB-231 cells with forced expression of STC1 and DROSHA silencing (**f**), and tumor volumes were monitored (**g**). Ctrl, control cells. **h** Secondary limited dilution xenograft was performed by plating gradually decreasing numbers of primary xenografted tumor cells into immunodeficient mice ($n = 5$, biological replicates) and calculated with ELDA analysis. **i** Representative images of DROSHA, STC1 and NANOG IHC staining in breast tumor specimens ($n = 58$, biological replicates). Scale bars, 100 μm or 50 μm. Data are shown as means ± SD. *P* values were calculated with two-tailed unpaired Student's *t*-test in **a**, **b**, **e**, **g**, ANOVA test in **d**, χ^2 test in **c**, **h**, Pearson's correlation test in **i**. $P < 0.05$ is considered statistically significant.

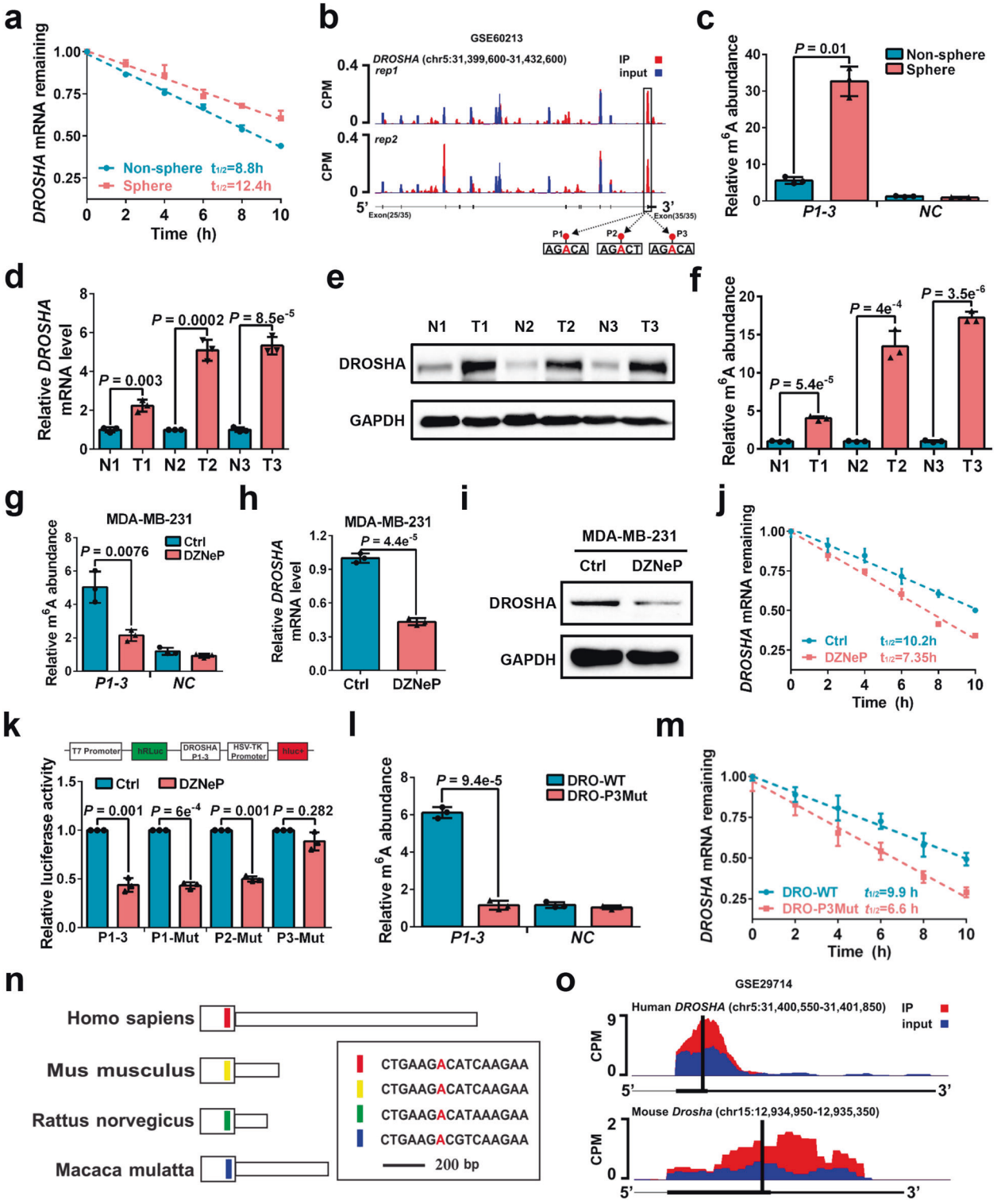

ubiquitylation (Fig. 4h). These data propose that AURKA protects METTL14 protein from ubiquitylation-degradation to promote *DROSHA* m^{6}A modification.

Next, we found that ablation of METTL14 significantly decreased DROSHA expression in breast cancer cells (Supplementary information, Fig. S6a, b). The available m^{6}A-sequence data revealed that depletion of METTL14 reduced m^{6}A peak near the *DROSHA* P3 motif in various cancer cells (Supplementary information, Fig. S6c, d). Similar reduction of *DROSHA* mRNA m^{6}A methylation was observed in the METTL14-knockdown MDA-MB-231 cells compared to controls in meRIP-qPCR assays (Fig. 4i). Accelerated *DROSHA* mRNA decay upon silencing METTL14 was confirmed in MDA-MB-231 cells (Fig. 4j). Furthermore, silencing of METTL14 reduced luciferase activity of the P1-3 reporter, but not that of the P3-Mut reporter in MDA-MB-231 cells (Fig. 4k). Moreover, R298P mutation (R298P) significantly reduced the m^{6}A methylation activity of METTL14 (Supplementary information, Fig. S6e, f), overexpression of WT METTL14 promoted luciferase

Fig. 3 *DROSHA* mRNA is stabilized by m^{6}A deposition. a Stability of *DROSHA* mRNA in non-sphere and sphere of MDA-MB-231 cells. mRNA levels were quantified by RT-qPCR. **b** UCSC Genome Browser plot containing tracks for m^{6}A-seq IP reads (red) and input reads (blue) at the *DROSHA* locus by analyzing meRIP-seq data (GSE60213). The sequence of m^{6}A motif near *DROSHA* stop codon is highlighted in three black boxes. **c** meRIP-qPCR was used to quantify relative *DROSHA* P1-3 m^{6}A levels in non-sphere or sphere of MDA-MB-231 cells. NC, negative control, the primer of *DROSHA* non-m^{6}A segment. **d**, **e** Relative mRNA (**d**) and protein (**e**) levels of *DROSHA* were determined between three breast tumor specimens and paired adjacent normal breast specimens. **f** meRIP-qPCR was used to quantify relative *DROSHA* m^{6}A levels in three breast tumor specimens and paired adjacent normal breast specimens. **g** meRIP-qPCR was used to quantify relative *DROSHA* P1-3 m^{6}A levels in MDA-MB-231 cells treated with DZNeP. **h**, **i** Relative mRNA (**h**) and protein (**i**) levels of *DROSHA* were determined in MDA-MB-231 cells treated with DZNeP. **j** Stability of *DROSHA* mRNA in MDA-MB-231 cells treated with DZNeP. **k** Relative luciferase activity of the *DROSHA* P1-3, P1-Mut, P2-Mut or P3-Mut reporter in HEK293T cells treated with DZNeP ($n = 3$, biological replicates). **l** meRIP-qPCR was used to quantify relative *DROSHA* P1-3 m^{6}A levels in MDA-MB-231 cells with forced expression of DRO-WT and DRO-P3Mut. **m** Stability of *DROSHA* mRNA in MDA-MB-231 cells by forced expression of DRO-WT and DRO-P3Mut. **n** Diagram of the last exon of *DROSHA* genes from various organisms including coding sequence (large box) and 3′UTR. The conserved sequences are indicated by colored boxes. **o** m^{6}A-seq reads cluster at the same distinct regions of DROSHA in both human brain RNA (top) and mouse brain RNA (bottom) by analyzing meRIP-seq data (GSE29714). Data are shown as means ± SD. *P* values were calculated with two-tailed unpaired Student's *t*-test and $P < 0.05$ is considered statistically significant.

activity of the P1-3 reporter but not P3-Mut reporter, while the R298P METTL14 had no effect on luciferase activity of either *DROSHA* reporters (Supplementary information, Fig. S6g). Clinically, METTL14 mRNA and protein were highly expressed in breast tumor compared with paired normal breast specimens (Supplementary information, Fig. S6h, i). In addition, WT, but not R298P, METTL14 rescued *DROSHA* mRNA m^{6}A level in AURKA-deficient cells (Fig. 4l). Importantly, WT, but not R298P, METTL14 partially restored luciferase activity of the P1-3 *DROSHA* (Fig. 4m) as well as DROSHA expression (Fig. 4n) following AURKA silencing. Taken together, these results reveal that AURKA enhances *DROSHA* mRNA stability partially via METTL14-dependent m^{6}A deposition in breast cancer cells.

AURKA strengthens IGF2BP2 binding to m^{6}A for *DROSHA* transcript stabilization

To further explore other mechanisms by which AURKA regulated *DROSHA* mRNA stability independent of the METTL14-regulated m^{6}A change, METTL14-overexpressing cells were established to determine whether a steady *DROSHA* m^{6}A state could be maintained following AURKA depletion. Indeed, AURKA knockdown had no effects on *DROSHA* m^{6}A levels in METTL14-overexpressing cells (Fig. 5a). However, ablation of AURKA attenuated *DROSHA* mRNA stability and decreased DROSHA expression in METTL14-overexpressing cells (Fig. 5b, c). As insulin-like growth factor 2 mRNA-binding proteins 1, 2 and 3 (IGF2BP1-3) have recently been reported as m^{6}A readers to recognize and stabilize m^{6}A modified transcripts,[16] we hypothesized that IGF2BP1-3 mediate AURKA-enhanced *DROSHA* stability in an METTL14-independent manner. We found that depletion of IGF2BP2, but not IGF2BP1 or 3, substantially reduced AURKA-regulated *DROSHA* mRNA stability in METTL14-overexpressing cells (Fig. 5d; Supplementary information, Fig. S7a–c). Ablation of IGF2BP2 also restricted AURKA-regulated DROSHA protein expression in METTL14-overexpressing cells (Fig. 5e). In addition, binding of IGF2BP2 to *DROSHA* transcript was enriched in sphere cells compared to non-sphere cells (Supplementary information, Fig. S7d). Both the mRNA and protein levels of IGF2BP2 showed no significant differences between breast tumor specimens and the paired normal breast specimens (Supplementary information, Fig. S7e, f).

We next investigated how IGF2BP2 mediated AURKA-enhanced *DROSHA* mRNA stability. The mass spectrometry result of AURKA-interacting proteins indicates that AURKA can interact with IGF2BP2 (Supplementary information, Table S4). As expected, AURKA and IGF2BP2 were colocalized in breast cancer cells (Fig. 5f). Co-immunoprecipitation (co-IP) results confirmed the cellular interaction between AURKA and IGF2BP2 (Fig. 5g, h). Furthermore, MD simulation unveiled 33 combinations of high interaction possibilities between amino acids of AURKA and IGF2BP2 (Fig. 5i), with the amino acids responsible for the AURKA and IGF2BP2 interaction (red color) displaying spatial proximity (Fig. 5j; Supplementary information, Movie S2). Direct interaction between AURKA and IGF2BP2 (1–220 amino acids) purified proteins was determined using in vitro interaction assay (Fig. 5k). In addition, co-localization of AURKA protein and *DROSHA* mRNA was observed in breast cancer cells (Fig. 5l; Supplementary information, Fig. S7g), which indicates that AURKA protein can bind to *DROSHA* mRNA. To verify this, we confirmed the binding of AURKA to *DROSHA* transcript by RNA immunoprecipitation (RIP) assay (Fig. 5m; Supplementary information, Fig. S7h). RNA pull-down results showed that amongst all antisense and sense RNA fragments, only the *DROSHA* L4 sense fragment pulled down AURKA protein from breast cancer cell lysates (Fig. 5n; Supplementary information, Fig. S7i).

As AURKA interacts with IGF2BP2 in an RNA-independent manner (Fig. 5g, h) and predominantly localizes in the nucleus in breast cancer cells,[18] we evaluated whether AURKA promotes nuclear translocation of IGF2BP2 to recognize m^{6}A modification. However, depletion of AURKA did not alter the cytoplasmic and nuclear distribution of IGF2BP2 (Supplementary information, Fig. S7j). Moreover, the IGF2BP2-binding *DROSHA* P3 m^{6}A motif is located in L5 region near the AURKA-binding L4 region, we reasoned that AURKA reinforced the binding of IGF2BP2 to the m^{6}A modification to stabilize *DROSHA* transcript. To validate this hypothesis, we performed AURKA knockdown and found decreased co-localization between IGF2BP2 protein and *DROSHA* mRNA in the nucleus (Supplementary information, Fig. S7k). Importantly, depletion of AURKA decreased m^{6}A levels in control cells but not in METTL14-overexpressing cells (Supplementary information, Fig. S7l), and diminished the capacity of IGF2BP2 binding to *DROSHA* mRNA in control cells (decreased by ~3.3 fold) more than in METTL14-overexpressing cells (decreased by ~1.7 fold) (Fig. 5o). In contrast, IGF2BP2 knockdown had little effect on the capacity of AURKA binding to *DROSHA* mRNA (Supplementary information, Fig. S7m). Altogether these findings confirmed that AURKA strengthens the binding of IGF2BP2 to the m^{6}A-modified transcript to stabilize *DROSHA* mRNA.

Suppression of *DROSHA* m^{6}A modification attenuates BCSC traits

We next evaluated the effects of *DROSHA* m^{6}A modification on BCSC phenotype. Overexpression of DRO-WT, but not the DRO-P3Mut, substantially rescued the ALDH$^+$ subpopulations in endogenous DROSHA-knockdown cells (Fig. 6a; Supplementary information, Fig. S8a, b). Consistently, forced expression of DRO-WT rather than DRO-P3Mut remarkably restored sphere formation ability in endogenous DROSHA-depleted cells using extreme limiting dilution assays and replating sphere formation assays (Fig. 6b–d). Endogenous DROSHA stably knocked down MDA-MB-231 cells or control cells with forced expression of DRO-WT or DRO-P3Mut were injected into nude mice ($n = 5$). Mice inoculated with overexpression of DRO-WT, but not DRO-P3Mut cells

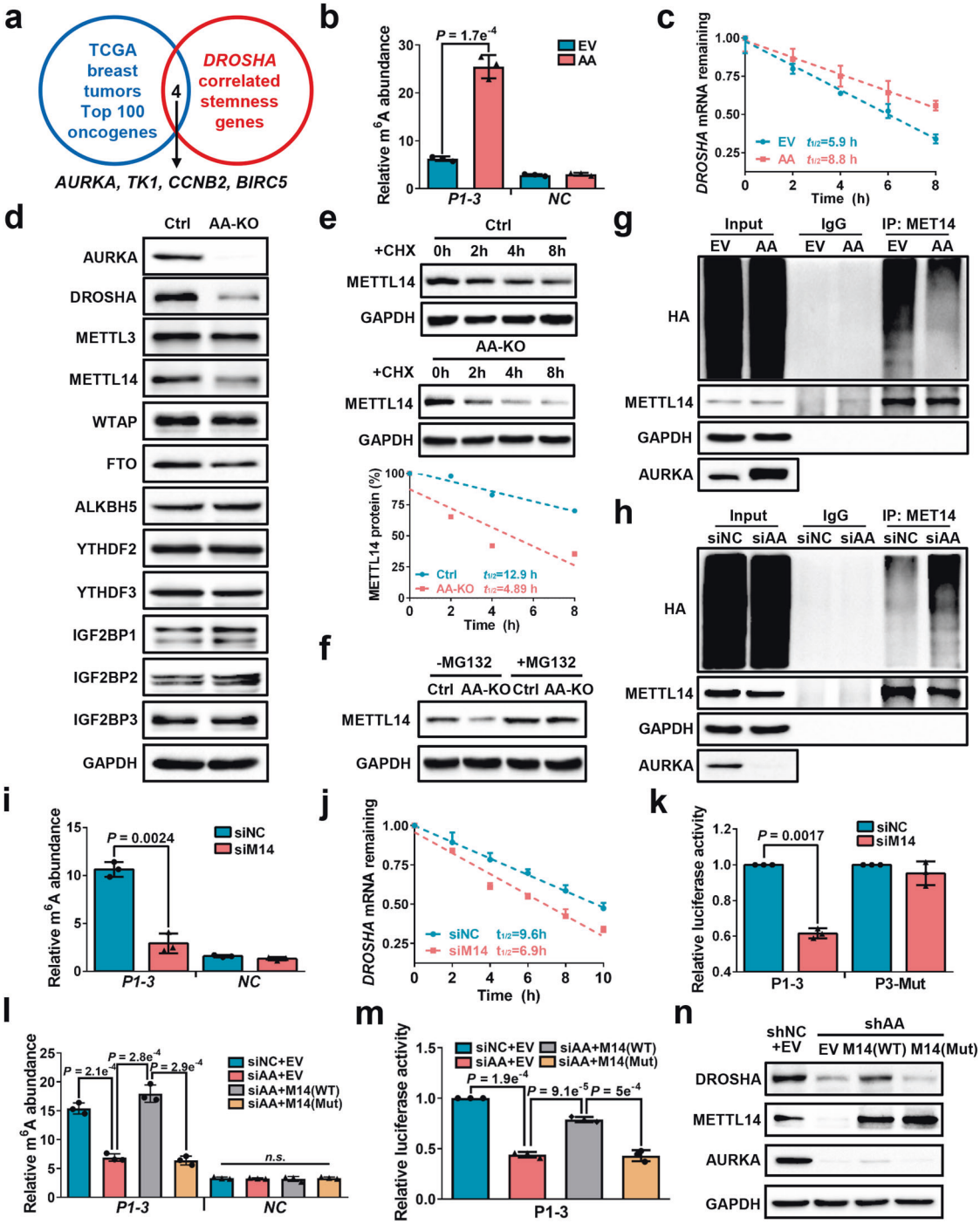

Fig. 4 AURKA-stabilized METTL14 maintains DROSHA transcript via m^{6}A deposition. a Comparison of *DROSHA*-correlated stemness genes with highly expressed oncogenes in TCGA breast tumor (top 100), common genes were listed. **b** meRIP-qPCR was used to determine relative *DROSHA* P1-3 m^{6}A levels in AURKA-overexpressing SK-BR-3 cells. EV, empty vector, AA, overexpression of AURKA. **c** Stability of *DROSHA* mRNA in AURKA-overexpressing SK-BR-3 cells. **d** The expression of indicated proteins was detected in AURKA-knockout MDA-MB-231 cells by western blotting. AA-KO, knockout of AURKA. **e** METTL14 expression was detected in AURKA-knockout MDA-MB-231 cells treated with cycloheximide (CHX, 200 μg/mL). METTL14 proteins were quantified by densitometry and plotted as a scatter diagram at the bottom. **f** METTL14 expression was detected in AURKA-knockout MDA-MB-231 cells treated with MG132 (10 μM) for 8 h. **g**, **h** HEK293T cells were transfected with indicated constructs (**g**) or siRNAs (**h**) followed by co-transfection with HA-Ub and METTL14 constructs. Cells were treated with MG132 (10 μM) for 8 h before collection. The whole cell lysate was subjected to immunoprecipitation with METTL14 antibody and western blotting with anti-HA antibody to detect ubiquitylated METTL14. **i** meRIP-qPCR was performed to verify relative *DROSHA* P1-3 m^{6}A levels in METTL14-knockdown MDA-MB-231 cells. **j** Stability of *DROSHA* mRNA in METTL14-knockdown MDA-MB-231 cells. **k** Relative luciferase activity of P1-3 and P3-Mut in HEK293T cells with METTL14 knockdown. **l** Relative *DROSHA* P1-3 m^{6}A levels were detected in AURKA-deficient MDA-MB-231 cells with or without overexpression of indicated METTL14. **m** Relative luciferase activity of P1-3 in AURKA-deficient HEK293T cells with or without indicated overexpression of METTL14. **n** DROSHA, METTL14 and AURKA protein expression was identified in AURKA-deficient MDA-MB-231 cells with or without overexpression of indicated METTL14. shAA, shRNA against *AURKA*. Data are shown as means ± SD. *P* values were calculated with two-tailed unpaired Student's *t*-test and $P < 0.05$ is considered statistically significant.

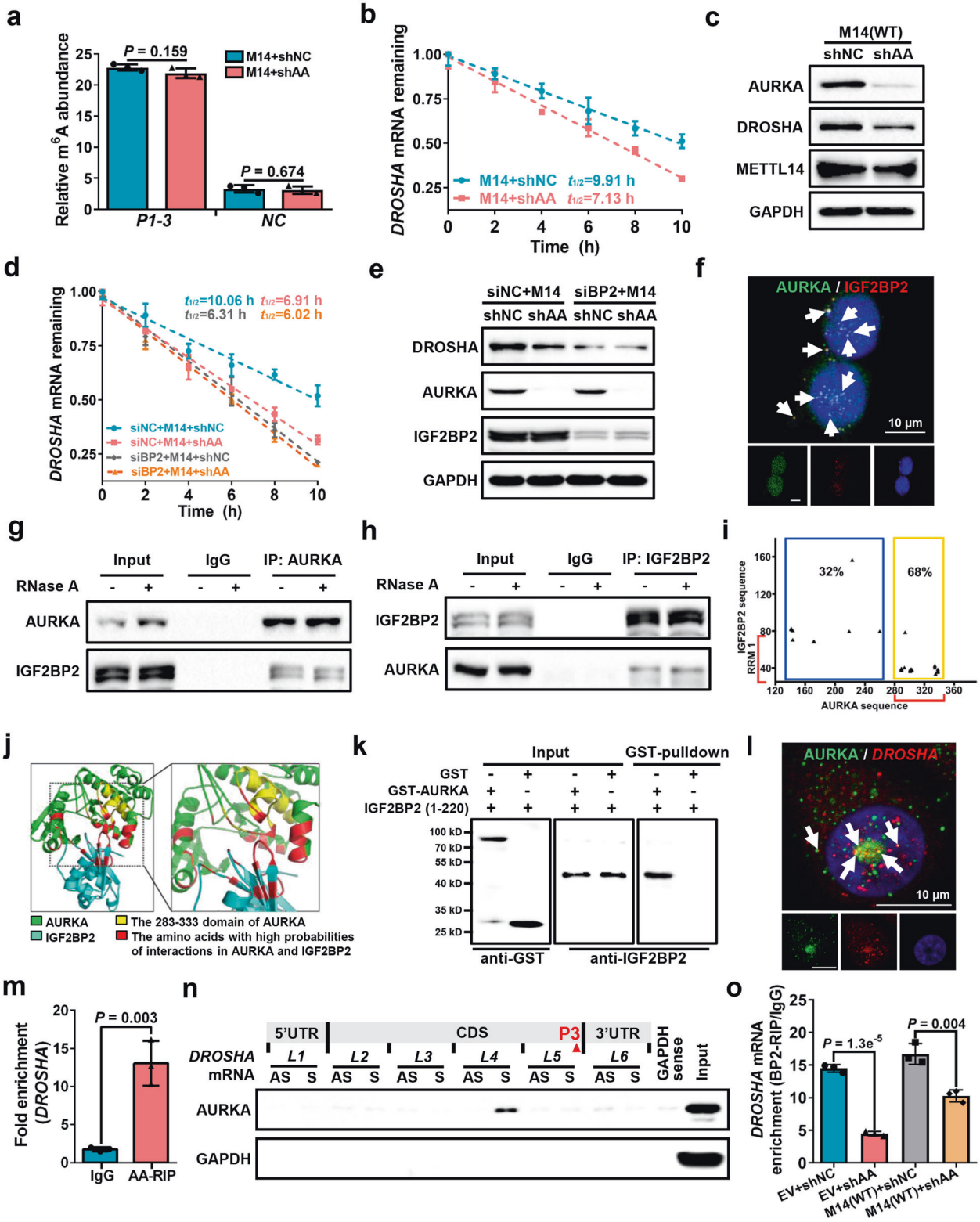

significantly increased the volume of tumor masses compared to the mice injected with DROSHA-deficient cells (Fig. 6e, f; Supplementary information, Fig. S8c). Furthermore, we found that the proportion of ALDH^{+} populations was decreased in breast cancer cells with DZNeP treatment (Fig. 6g; Supplementary information, Fig. S8d). DZNeP also inhibited sphere formation ability in extreme limiting dilution assays (Fig. 6h). Similarly, treatment with DZNeP significantly decreased the diameter and number of spheres in breast cancer cells using replating sphere formation assay (Fig. 6i, j; Supplementary information, Fig. S8e, f). In addition, MDA-MB-231 cells were injected into nude mice treated with DZNeP each day during the tumor measurement. Mice treated with DZNeP evidently formed smaller tumor masses compared to the mice injected with normal saline (Fig. 6k, l).

Fig. 5 AURKA strengthens IGF2BP2 binding to m^{6}A for DROSHA transcript stabilization. a meRIP-qPCR was performed to verify relative *DROSHA* P1-3 m^{6}A levels in METTL14-overexpressing MDA-MB-231 cells with or without AURKA-deficiency. **b** Stability of *DROSHA* mRNAs were identified in METTL14-overexpressing MDA-MB-231 cells with or without AURKA-deficiency. **c** The protein expression of AURKA, DROSHA and METTL14 was identified in METTL14-overexpressing MDA-MB-231 cells with or without AURKA deficiency. **d** Stability of *DROSHA* mRNAs was evaluated in METTL14-overexpressing plus IGF2BP2-knockdown (siIGF2BP2) or siNC MDA-MB-231 cells with or without AURKA deficiency. **e** DROSHA, AURKA and IGF2BP2 proteins were detected by western blotting in METTL14-overexpression plus siIGF2BP2 or siNC MDA-MB-231 cells with or without AURKA deficiency. **f** The representative image of co-staining of AURKA protein (green) and IGF2BP2 protein (red) were observed in MDA-MB-231 cells. The nucleus was stained by DAPI (blue). Scale bars, 10 μm. **g**, **h** Co-IP assay to identify the endogenous interaction between AURKA and IGF2BP2 in MDA-MB-231 cells. Cell extracts were untreated (–) or treated (+) with RNase A (50 mg/mL). **i** The dot plot represents the amino acids in orange box located in the nucleotide 283–333 region of the AURKA sequence and the RRM region of the IGF2BP2 sequence. **j** The simulated interaction diagram of AURKA and IGF2BP2. **k** Direct interaction between GST-AURKA fusion protein and recombinant IGF2BP2 (1–220) protein was determined by in vitro interaction assay. **l** The representative image of co-staining (indicated by white arrows) of AURKA protein (green) and *DROSHA* mRNA (red) observed in the nucleus (blue). Scale bars, 10 μm. **m** Levels of AURKA-binding to *DROSHA* mRNA were determined by RIP assay in MDA-MB-231 cells. **n** Proteins in MDA-MB-231 cells pulled down by the indicated biotin-RNAs were analyzed with AURKA antibody. AS, antisense; S, sense. **o** Levels of IGF2BP2 binding to *DROSHA* mRNA were determined by RIP assay with or without AURKA-deficiency in control MDA-MB-231 cells or METTL14-overexpressing MDA-MB-231 cells. Data are shown as means ± SD. *P* values were calculated with two-tailed unpaired Student's *t*-test and $P < 0.05$ is considered statistically significant.

Taken together, these results reveal that blockage of *DROSHA* m^{6}A modification significantly inhibits BCSC phenotype.

DISCUSSION

DROSHA, a catalytic subunit of the microprocessor complex, has been shown to be dysregulated during tumorigenesis.[6] However, the aberrant regulatory network of DROSHA in promoting BCSC property remains elusive. Here, we demonstrate a non-canonical function of DROSHA to transactivate *STC1* through interacting with β-Catenin in BCSCs. Oncogenic AURKA enhances m^{6}A-dependent *DROSHA* mRNA stability through (1) stabilizing METTL14 by inhibition of ubiquitylation-mediated degradation and (2) strengthening IGF2BP2 to stabilize m^{6}A-modified *DROSHA* transcript. Indeed, WT DROSHA, but not an m^{6}A methylation-deficient mutant, enhance BCSC stemness, whereas inhibition of *DROSHA* m^{6}A modification suppresses tumor growth. Clinically, both DROSHA and STC1 predict adverse prognosis of breast cancer patients. Moreover, *DROSHA* m^{6}A level is positively correlated with the expression of DROSHA and METTL14 enriched in breast tumor tissues. Thus, we unveil the AURKA-induced oncogenic m^{6}A modification in stabilizing *DROSHA* transcript and identify a novel DROSHA transcriptional function in promoting BCSC phenotype.

The regulation of miRNAs by DROSHA is widely involved in tumor development[5]. Interestingly, our GSEA reveals that positively regulated targets by DROSHA are enriched in the CD44$^+$/CD24$^-$ BCSC subpopulations, indicating that besides its conventional role in RNA processing, DROSHA transcriptionally enhances stemness factors to maintain BCSCs. Previous studies have shown that DROSHA binding with promoter-proximal regions to regulate human gene transcription by associating with the RNA-binding protein CBP80 and RNA Polymerase II.[8] In this study, DROSHA interacts with β-Catenin to promote *STC1* transcription in breast cancer cells. The CED domain (390–875 amino acids) of DROSHA is responsible for its interaction with β-Catenin to transactivate *STC1*, which represents a novel mechanism of the transcriptional function for DROSHA. In addition, STC1 has recently been shown to promote stem-like traits in glioblastoma cells.[26] Consistently, STC1 functions downstream of DROSHA to maintain BCSCs, as overexpression of STC1 rescues the DROSHA-repressed BCSC phenotype.

DROSHA mRNA is transcriptionally regulated by c-Myc and E2F1 to promote miRNA processing in B lymphoma and lung cancer cells,[9,27] whereas the potential mechanism by which *DROSHA* mRNA stability is regulated has hitherto remained unknown. Accumulated studies reveal that m^{6}A modification can either enhance or attenuate mRNA stability dependent on the type of m^{6}A reader protein[11]. YTHDF2 targets thousand m^{6}A-modified transcripts to promote mRNA decay.[28] Conversely, IGF2BPs selectively recognize m^{6}A-modified transcript to promote mRNA stability.[16] In our study, m^{6}A modification is enriched near the *DROSHA* mRNA stop codon, consistent with the findings that DROSHA expression is much higher in breast tumor tissues. Inhibition of m^{6}A modification or mutation of the m^{6}A site attenuates the stability of *DROSHA* mRNA, which uncovers a novel regulatory mechanism of *DROSHA* mRNA stability. Furthermore, RNA m^{6}A methylation has been shown to be required for cancer initiation and progression in numerous solid tumors and acute myeloid leukemia.[29,30] As DZNeP has been reported as an RNA methylation inhibitor in both normal and cancer cells,[24] we find that DZNeP inhibits *DROSHA* m^{6}A methylation and effectively attenuates BCSC traits. On the other hand, DZNeP as the first nonspecific EZH2 inhibitor has been used to mediate several antitumor activities including inhibition of biliary tract cancer stem cells through repression of PRC2 and removal of H3K27me3 marks,[31,32] which implies another possibility that DZNeP might suppress BCSC properties through inhibition of histone methylation.

The mechanistic roles of m^{6}A methyltransferases have been substantially investigated during cancer progression. For example, METTL14 elevates the expression of oncogenic *MYB* and *MYC* via m^{6}A modification to promote AML development and LSC self-renewal[14]. Reductions in m^{6}A methylation due to either METTL14 mutation or reduced expression of METTL3 promote tumorigenicity through activation of the AKT pathway.[33] Although recent study reveals that SUMOylation of METTL3 is critical for m^{6}A methyltransferase activity in lung cancer,[34] how the m^{6}A methyltransferase METTL14 is controlled during cancer progression has remained enigmatic. Previously, we show that AURKA locates preferentially into nucleus to transactivate *MYC* in a kinase-independent manner.[18] In the present work, we find that inhibition of AURKA kinase activity has no impacts on METTL14 expression. Yet, we uncover a novel role of the oncogenic AURKA in stabilizing METTL14 protein through suppressing ubiquitylation-dependent degradation, another kinase-independent role of AURKA in regulating protein stability.

The presence or absence of association partners might account for the variable distribution of m^{6}A readers, such as YTHDF2, contributing to different biological functions.[35] How diverse readers achieve selectivity toward certain m^{6}A sites or certain m^{6}A-modified transcripts remains elusive. One likely scenario is that readers may be localized to different regions of mRNA through interacting with other RNA binding proteins (RBPs) that recognize distinct features of the RNA.[36] In concordance, we find that the RBP-like AURKA binds to *DROSHA* transcript near the *DROSHA* m^{6}A site and strengthens the binding of IGF2BP2 to m^{6}A modification for *DROSHA* stability. We speculate that AURKA likely

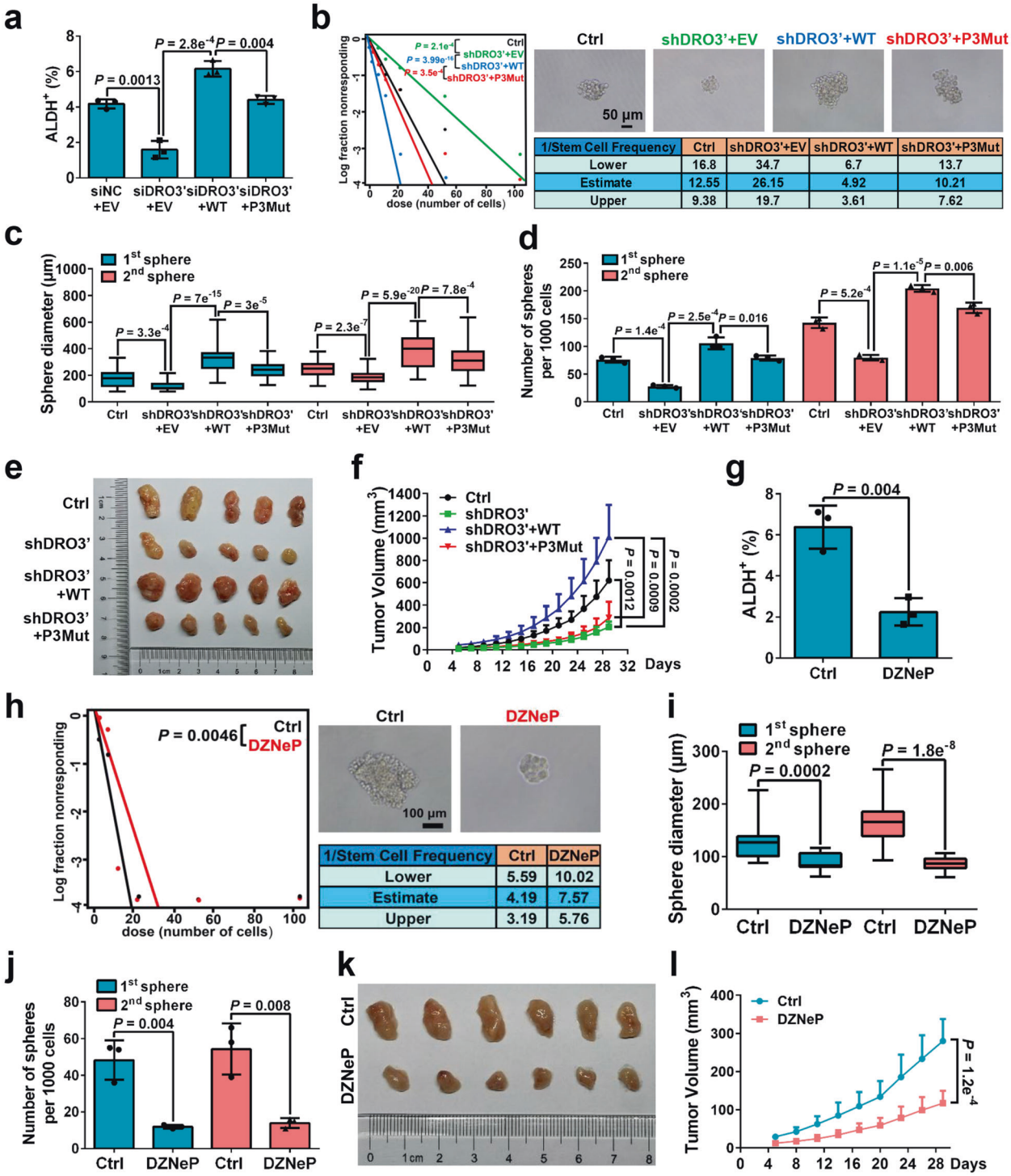

acts as a 'locker' or 'harness' to strengthen IGF2BP2 binding to the m^{6}A modification and subsequently stabilize the *DROSHA* transcript. Similar notion was raised in a recent study revealing that SMAD2/3 promotes binding of the m^{6}A methyltransferase complex METTL3-METTL14-WTAP to a subset of transcripts involved in early cell fate decisions.[37] In addition, the KH3-4 domains are critical for the binding of IGF2BPs to m^{6}A-modified RNAs. However, KH3-4 peptides alone showed poor selectivity and affinity for m^{6}A RNA compared with full-length proteins, indicating that other mechanisms may be involved in the recognition of m^{6}A by the KH domains of IGF2BPs.[16] Thus, it is possible that AURKA directly interacting with N-terminal RRM domains of IGF2BP2 might further alter the conformation of KH3-4 domains, leading to preferential recognition of m^{6}A. This hypothesis is worth further investigation in the future study. Hence, this dual function of the oncogenic AURKA represents a novel and intriguing mechanism of oncogenic m^{6}A epigenetic modification in BCSC maintenance.

Collectively, our results reveal that DROSHA interacts with β-Catenin to transactivate *STC1* in a non-canonical fashion, contributing to BCSC phenotype. The AURKA/METTL14/IGF2BP2-regulated oncogenic m^{6}A modification enhances the mRNA stability of *DROSHA* to maintain its high expression levels in

Fig. 6 Suppression of DROSHA m^{6}A modification attenuates BCSC traits. a ALDH$^+$ populations were analyzed following endogenous DROSHA knockdown and forced expression of WT or P3Mut DROSHA in MDA-MB-231 cells. siDRO3′, siRNA against *DROSHA* 3′UTR. **b** Left: ELDA was performed in MDA-MB-231 cells with endogenous DROSHA knockdown and forced expression of WT or P3Mut DROSHA. Top right: The representative sphere images are shown. Scale bars, 50 μm. Bottom right: Stemness frequency illustration of the cells with the upper and lower 95% confidence intervals meaning that the frequency of one stem cell in cancer cells. shDRO3′, shRNA against *DROSHA* 3′UTR. Spheres were counted from 24 replicate wells. **c**, **d** Replating sphere formation was performed in MDA-MB-231 cells with endogenous DROSHA knockdown and forced expression of indicated DROSHA. The diameter (**c**) and number (**d**) of spheres were quantified. Spheres were counted from three replicate wells. The diameter and number of each experiment represent the total count of three replicate wells. **e**, **f** Immunodeficient mice ($n = 5$, biological replicates) were subcutaneously inoculated with MDA-MB-231 cells with endogenous DROSHA knockdown and forced expression indicated DROSHA (**e**), and tumor volumes were monitored (**f**). **g** ALDH$^+$ populations were analyzed in MDA-MB-231 cells treated with DZNeP. **h** Left: ELDA was addressed in MDA-MB-231 cells treated with DZNeP. Top right: The representative sphere images are shown. Scale bars, 100 μm. Bottom right: Stemness frequency illustration of the cells with the upper and lower 95% confidence intervals meaning that the frequency of one stem cell in cancer cells. Spheres were counted from twenty-four replicate wells. **i**, **j** Replating sphere formation was performed in MDA-MB-231 cells treated with DZNeP. The diameter (**i**) and number (**j**) of spheres were quantified. Spheres were counted from three replicate wells. The diameter and number of each experiment represent the total count of three replicate wells. **k**, **l** Immunodeficient mice ($n = 6$, biological replicates) were subcutaneously inoculated with MDA-MB-231 cells treated with DZNeP (**k**), and tumor volumes were measured (**l**). Data are shown as means ± SD. *P* values were calculated with two-tailed unpaired Student's *t*-test in **a**, **d**, **f**–**g**, **j**, **l**, *ANOVA* test in **c** and **i**, χ^2 test in **b**, **h**. $P < 0.05$ is considered statistically significant.

BCSCs. Targeting m^{6}A modification of *DROSHA* represents a novel therapeutic approach for breast malignancies (Supplementary information, Fig. S8g).

MATERIALS AND METHODS

Cell culture and breast tissue specimens

The human breast cancer cell lines, MDA-MB-231 (HTB-26), SK-BR-3 (HTB-30), BT549 (HTB-122) and MCF-7 (HTB-22) purchased from American Type Culture Collection (ATCC) were, respectively, cultured in Leibovitz's L-15 Medium (Gibco, 11415056), McCoy's 5A Modified Medium (Gibco, 16600082), RPMI-1640 Medium (Gibco, 11876093) containing 0.023 IU/mL insulin (Sigma, 91077C) and Eagle's Minimum Essential Medium (Gibco, 11095080) containing 0.01 mg/mL human recombinant insulin (Sigma) with 10% fetal bovine serum (FBS, Gibco, 10100147), 0.1% penicillin-streptomycin (Thermo, 15140122) and anti-mycoplasma reagent SaveIt (Hanbio, HB-SV1000). HEK293T (CRL-11268) cells from ATCC were grown in dulbecco's modified eagle medium (Gibco, 10569044) containing 10% FBS, 0.1% penicillin-streptomycin (Thermo) and SaveIt. All cells were maintained at 37 °C in a humidified 5% CO_2 atmosphere except MDA-MB-231 cultured in atmospheric air and were not cultured continuously for more than 3 months. Cryopreservation of all cell lines were using CELLSAVING (New Cell & Molecular Biotech, C40100). All cell lines were authenticated by STR profiling and tested for mycoplasma contamination with the method of PCR. Petri dishes and cell culture plates were purchased from Guangzhou Jet Bio-Filtration Co., Ltd.

Twenty-one pairs of breast tumor specimens and conjugate breast normal specimens were obtained from the same patients undergoing surgery, following informed consent from patients and approved by the Institutional Ethics Review Board of the Second Affiliated Hospital of Dalian Medical University (No. 2019-028). The clinical information of breast cancer patients was listed in Supplementary information, Table S5.

Transfection, lentivirus package and stable cell line generation

Transient transfection with siRNAs (GenePharma, Suzhou, China) or plasmids was performed using Lipofectamine 3000 (Lipo3000, Invitrogen, L3000015) according to the manufacturers' protocols. Lentivirus was packaged in HEK293T cells using the second-generation packaging system plasmids psPAX2 (Addgene plasmid, #12260) and pMD2.G (Addgene plasmid, #12259). HEK293T cells were seeded in a 6-well plate to allow 80% confluency in the next day. Lentiviral plasmid (pLVX-STC1 or pLVX-METTL14), psPAX2 and pMD2.G were co-transfected into HEK293T cells using Lipo3000. Supernatants were collected every 24 h between 48 and 72 h after transfection and the viral titer was determined. Lentiviral-mediated short hairpin RNA (shRNA) directed against DROSHA were purchased from GenePharma, Suzhou, China. All siRNA and shRNA sequences were listed in Supplementary information, Table S1.

For lentiviruses infection, cells were infected and subsequently selected in the presence of 2 μg/mL puromycin (Sigma, P8833) for over 72 h. MDA-MB-231 (Tet-on shAURKA) cells was achieved in our previous study.[18]

To construct the AURKA-knockout cell line, we used one vector CRISPR-Cas9 genome editing system (lentiCRISPR v2, Addgene #52961) to generate an AURKA knockout cell line in MDA-MB-231 cells following the manufacturer's protocols.[38] The gRNA sequence targeting AURKA was 5′-TGAGTCACGAGAACACGTTT-3′.

Plasmid construction

DRO-WT was subcloned into pcDNA6b vector. WT, amino acid truncation (1–875 and 876–1374, D875) DROSHA. WT β-Catenin was subcloned into pcDNA6b vector with His tag. m^{6}A-enriched fragment of DROSHA (P1-3) was subcloned into psiCHECK2 vector. WT METTL14 and WT STC1 were subcloned into pLVX-DsRed-Monomer-N1. WT and truncated 500, 1000, 1500 bp (D500, D1000, D1500) promoters of STC1 were subcloned into pGL3-Basic vectors. *STC1* and *DROSHA* promoters were subcloned into pLVX-OS-dGFP vectors. Plasmids of psiCHECK2-DROSHA (P1-Mut, P2-Mut and P3-Mut), pLVX-METTL14 (R298P, catalytic mutant), pcDNA6-DROSHA (E1045Q, RNase III domain mutant), pcDNA6-DROSHA (P3Mut, m^{6}A site mutant), pGL3-STC1 (Mut1, Mut2 and Mut1 plus Mut2, predicted TCF-bind sites mutant) were generated by site-directed mutagenesis using PCR. WT AURKA was subcloned into pGEX-6P-1 vector with His tag. All the primers used for plasmid construction are listed in Supplementary information, Table S1. pcDNA6b-Flag-AURKA was established in our previous study.[18] pcDNA6b-MYC was established in our previous study.[39] HA-Ub was a gift from Prof. Lingqiang Zhang lab (Beijing Institute of Lifeomics, Beijing, China).

RNA extraction and RT-qPCR

Total RNAs were extracted using AG RNAex Pro Reagent (AG21101, ACCURATE BIOTECHNOLOGY, HUNAN) or RNAiso Plus (TaKaRa, 9109) according to the manufacturer's instructions, which were used to generate cDNA using EasyScript One-Step gDNA Removal and cDNA Synthesis SuperMix (TransGen Biotech, AE311-02) or Evo M-MLV RT Kit with gDNA Clean for qPCR (AG11705, ACCURATE BIOTECHNOLOGY, HUNAN). RT-qPCR using ChamQ^{TM} Universal SYBR qPCR Master Mix (Vazyme Biotech Co., Ltd, Q711-02) was performed on a Real-time PCR System (Agilent Technologies Stratagene Mx3005P). *ACTB* or *GAPDH* was used as an internal control to normalize RNA expression. The primers used in RT-qPCR were shown in Supplementary information, Table S1.

m^{6}A dot blot

Total RNAs were extracted with RNAiso Plus (TaKaRa). Then, intact mRNAs were purified from total RNAs using Dynabeads mRNA purification kit (Ambion, 61006). The indicated amount of purified mRNA was denatured in 10 μL volume of RNA incubation buffer (50% formamide, 2.5% formaldehyde and 0.5× MOPS) at 55 °C for 15 min, followed by chilling on ice. RNA samples were applied to Amersham Hybond-N$^+$ membrane (GE Healthcare, RPN303B) with a Bio-Dot Apparatus (Bio-Rad). After UV crosslinking, the membrane was stained with 0.02% methylene blue (MB) in 0.3 M sodium acetate. The membrane was then washed with 1× PBST buffer, blocked with 5% non-fat milk in PBST, and incubated with anti-m^{6}A antibody (Synaptic Systems, #202003) overnight at 4 °C. After incubating with Goat anti-Rabbit IgG (H + L) Secondary Antibody (Thermo Fisher Scientific, 31460), the membrane was incubated using WesternBright ECL kit (Advansta, K-12045-D50) for chemiluminescent reading on ChemiDoc System (Bio-Rad).

Met depletion and DZNeP treatment

For Met depletion, cells were washed twice by Dulbecco's Phosphate Buffer Saline (0.137 M NaCl, 2.7 mM KCl, 1.1 mM KH_2PO_4, 0.5 mM $MgCl_2$, 8.1 mM Na_2HPO_4, 0.9 mM $CaCl_2$, pH 7.4), and then supplemented with Met-free media (Thermo Fisher, 21013024) to decrease m^{6}A level. For DZNeP treatment, cells were managed with 10 μM DZNeP (Selleck, S7120) to inhibit m^{6}A modification. In animal model, the mice were subcutaneously injected with DZNeP (8 mg/kg per mice) in each two days.

RNA stability assay

Breast cancer cells were transfected with plasmids or treated by DZNeP or methionine deprivation for 24 h. Then, cells were treated with 5 μg/mL actinomycin D (ActD, Sigma, CA1201) and collected at the indicated time points. The total RNAs were extracted by RNAiso Plus (TaKaRa) and analyzed by RT-qPCR.

Western blotting

Cells were lysed using RIPA buffer (50 mM Tris, pH 7.5, 120 mM NaCl, 1% Triton X-100, 0.5% Sodium Deoxycholate, 0.1% SDS, 5 mM EDTA) with protease inhibitor cocktail (MedChemExpress, HY-K001) for 30 min. After centrifugation, supernatant was collected and boiled with 6× loading buffer. Equal amounts of proteins were loaded and separated by SDS-PAGE, transferred to nitrocellulose membranes (Millipore, HATF00010), incubated with primary and secondary antibodies. The membrane was incubated using WesternBright ECL kit for chemiluminescent reading on Bio-Rad. Here are antibodies used for western blotting: DROSHA (3364S), C-MYC (9402S), Phospho-Aurora A (T288) (3079S), Histone H3 (9715S), FTO (14386S) and GST (2625S) were purchased from Cell Signaling Technology (CST) in MA, USA. OCT4 (GTX101497) and NANOG (GTX100863) were from GeneTex in Southern California, USA. GAPDH (60004-1-ZJ), Beta-Actin (66009-1-Ig), GRB10 (23591-1-AP), SLCO4A1 (26399-1-AP), SORBS2 (24643-1-AP), METTL3 (15073-1-AP), METTL14 (26158-1-AP), WTAP (60188-1-IG), YTHDF2 (24744-1-AP), YTHDF3 (25537-1-AP), IGF2BP1 (14642-1-AP), IGF2BP2 (11601-1-AP), IGF2BP3 (22803-1-AP) and HA Tag (66006-2-Ig) were from Proteintech Group in Wuhan, China. β-Catenin (06-734), Aurora A (07-648) and ALKBH5 (ABE547) were from Millipore in MA, USA. STC1 (ab229477) was from Abcam in Cambridgeshire, UK. PARP (sc-8007) was from Santa Cruz Biotechnology in CA, USA. Goat anti-Rabbit IgG (H + L) Secondary Antibody (31460) and Goat anti-Mouse IgG (H + L) Secondary Antibody (31430) were purchased from Thermo Fisher Scientific, MA, USA.

meRIP-seq data analysis

meRIP-seq data were analyzed according to the protocol described previously.[40] In brief, reads underwent a set of QC checks with FastQC and Fastp, then were mapped to the reference genome (hg19 and mm10) with STAR. Mapped reads were provided as input for Deeptools and MACS2, which identified m^{6}A peaks adapted for visualization on the UCSC genome browser. The meRIP-seq data of GSE60213, GSE29714, GSE90642 and GSE54365 were used in this study.

mRNA purification and meRIP-qPCR

Total RNAs were extracted with RNAiso Plus (TaKaRa). Then, intact mRNAs were purified from total RNAs using Dynabeads mRNA purification kit (Ambion, 61006). For meRIP, the procedure was described previously.[41] In brief, purified mRNAs (5 μg) were digested by DNase I (M0303, NEB) and then fragmented into around 200-nt fragments by incubation at 95 °C for 25 s in RNA Fragmentation Reagents (Ambion, AM8740), followed by standard ethanol precipitation and collection. Anti-m^{6}A antibody (10 μg antibody for 5 μg mRNAs; Synaptic Systems) was incubated with 40 μL Protein A beads (Sigma, P9424) in IPP buffer (150 mM NaCl, 0.1% NP-40, 10 mM Tris-HCl, pH 7.4) for 2 h at room temperature. The fragmented mRNAs (5 μg) were incubated with the prepared antibody-bead mixture for 4 h at 4 °C. By washing three times, bound RNA was eluted from the beads with 0.5 mg/mL N^6-methyladenosine (BERRY & ASSOCIATES, P3732) in IPP buffer. The eluted RNA was extracted by EnoI:Chloroform:Isoamylol (pH < 5.0, Solarbio life science, P1025) and then generated to cDNA using 5× All-In-One RT MasterMix (ABM, G490). The enrichment of m^{6}A was quantified by qPCR. The sequences of qPCR primers are listed in Supplementary information, Table S1.

Dual-luciferase reporter assay

To measure the gene transcriptional activation, pGL3-STC1 (WT, D500, D1000, D1500, Mut1, Mut2 and Mut1 plus Mut2) reporter plasmids (Fluc) and renilla luciferase (Rluc) control plasmids (pRL-TK) were co-transfected with other plasmids or siRNAs in HEK293T cells. After 24 h, Fluc and Rluc activities were measured with the Dual-Luciferase Reporter Assay System (Promega, E1910) according to the manufacturer's instructions. The relative luciferase activity was calculated by dividing Fluc by Rluc and normalized to individual control for each assay.

To determine the RNA stability, psiCHECK2-DROSHA (WT, P1-Mut, P2-Mut and P3-Mut) reporter plasmids were co-transfected with other plasmids, siRNAs or treated by DZNeP or methionine deprivation. The activities of the renilla and firefly luciferases were quantified with the Dual-Luciferase Reporter Assay System after 24 h. The relative luciferase activity was calculated by dividing Rluc by Fluc and normalized to individual control for each assay.

Fluorescence in situ hybridization-immunofluorescence

Cells were mounted on the Circle Microscope Cover Glass (NEST, 801009). After fixation with 3.6% paraformaldehyde (Solarbio, P1110) and 10% acetic acid (Kermel, 6762007) for 15 min at room temperature, cells were pre-hybridized at 55 °C for 2 h and hybridized overnight at 55 °C in a humidified chamber with DIG-labeled UTP (Roche, 11277073910) nucleic acid probes. Post-hybridized glasses were stringently washed with 50% formamide/2× SSC (20× SSC, 3.0 M NaCl, 0.3 M sodium citrate, pH 7.0). The hybridization was visualized using anti-digoxygenin (1:100, Roche) and Alexa FlourTM 555 donkey anti-sheep IgG (1:200, Thermo Fisher Scientific). The protein was visualized using anti-AURKA antibody (1:100, Abcam) or anti-IGF2BP2 antibody (1:100, Proteintech Group) and Alexa FlourTM 488 donkey anti-rabbit IgG (1:200, Thermo Fisher Scientific). Nuclei were counterstained with DAPI. Image acquisition and analysis were addressed in the confocal microscope (Leica, TCS SP5II).

DROSHA probes were transcripted from DROSHA PCR fragments with T7 promoter in vitro with MEGAscript™ T7 Transcription Kit (Thermo Fisher Scientific, AM1333) and purified with RNAiso Plus (TaKaRa). Primers used to prepare DROSHA PCR fragments were listed in Supplementary information, Table S1.

RIP assay
Endogenous RIP studies were performed using the MagnaRIP Kit according to the manufacturer's protocol (Millipore, 17-700). Briefly, cells were lysed with RIP lysis buffer for 30 min on ice. The whole-cell lysates were incubated at 4 °C overnight with magnetic protein A-protein G beads coupled with 5 μg of either normal IgG antibody (Millipore) or AURKA antibody (Sigma, A1231), IGF2BP2 antibody (Proteintech, 11601-1-AP). Beads were then washed three times and incubated with proteinase K buffer (30 min at 55 °C). The co-precipitated RNAs were extracted with Enol:Chloroform:Isoamylol (pH < 5.0, Solarbio life science) and detected by RT-qPCR. The primers were listed in Supplementary information, Table S1.

Cytoplasmic and nuclear protein extraction
Cytoplasmic extracts were collected by resuspending the cell pellets in hypotonic buffer (20 mM Tris-HCl pH 7.4, 10 mM NaCl, 3 mM $MgCl_2$) supplemented with protease inhibitor (cocktail) and then were incubated on ice for 15 min. Next, 0.9% NP-40 (final concentration) was added with vortexing for 10 s and then were centrifuged for 10 min at 3000 rpm at 4 °C. The supernatants were transferred to new prechilled Ep tube. The residual pellets were washed with hypotonic buffer for 3 times and the supernatants were discarded thoroughly. To achieve nuclear extraction, the nuclear pellets were treated with nuclear extraction buffer (100 mM Tris-HCl, pH 7.4, 2 mM Na_3VO_4, 100 mM NaCl, 1% TritonX-100, 1 mM EGTA, 0.1% SDS, 1 mM NaF, 20 mM $Na_4P_2O_7$). After vortexing at every 10 min for 30 min at 4 °C, the lysates were centrifuged at 14,000 × *g* for 30 min at 4 °C. Supernatants after this spin contained the nuclear protein fraction.

Protein co-IP and LC-MS/MS analysis
Cells grown in 15-cm dishes at 70%–80% were lysed with co-IP buffer (50 mM Tris, pH 7.4, 150 mM NaCl, 1% NP-40, 0.5% sodium deoxycholate, 0.1% SDS, 1 mM phenylmethyl sulfonyl fluoride, protease cocktail), and collected by cell scrapers. Pull-downs were carried out in RNase A untreated lysates, except Fig. 5g, h, where 50 mg/mL RNase A was used to treat cell lysates during the pull-down procedure. Equal volume of lysates was respectively incubated with AURKA antibody (Sigma, A1231), IGF2BP2 antibody (Proteintech, 11601-1-AP), β-Catenin antibody (Millipore, 06-734), DROSHA antibody (CST, 3364 S), Flag-Tag antibody (Proteintech, 20543-1-AP), His-Tag antibody (CST, 12698), METTL14 antibody (Abcam, 252562) and the corresponding mouse IgG antibody (CST, 7076) or rabbit IgG antibody (CST, 7074). After applying a centrifugation, proteins associated with Protein A/G Plus-Agarose beads (Santa Cruz Biotechnology, SC-2003) were washed three times and analyzed by western blotting.

For mass spectrometry analysis, samples from immuno-enrichment with AURKA, DROSHA or IgG antibodies were loaded onto separated lanes of a 10% SDS polyacrylamide gel, then electrophoresed for 20 min. The entire gel region containing the proteins was cut from the gel and subjected to in-gel trypsin digestion and subsequent recovery of peptides as described previously.[42] LTQ-Orbitrap Elite (Thermo Scientific) coupled with Dionex UltiMate 3000 RSLCnano system (Thermo Scientific) was used for all proteomic analyses. The MS data were analyzed by Q-Exactive mass spectrometer and searched against the Uniprot human database by using the MaxQuant (version 1.6.0.1) software for peptide and protein identifications. A summary of the identified proteins can be found in Supplementary information, Tables S2 and S4.

Recombinant protein purification and in vitro interaction assay
AURKA protein was purified from BL21 *E. coli* that was transformed with pGEX6P1-GST-AURKA-His. Bacteria expressing GST-AURKA or GST were then lysed by sonication with 1 mg/mL lysozyme in PBS and 200 mM KCl. GST proteins were purified via magnetic glutathione affinity (V8611, Promega Corporation) and eluted in 50 mM Tris (pH 8.0) with 10 mM glutathione. Commercial recombinant human protein IGF2BP2 (1-220) was purchased from Novoprotein Scientific Inc (Q9Y6M1).

For in vitro interaction assay, recombinant IGF2BP2 (1-220) protein (5 μg) was incubated with 30 μL magnetic glutathione particles adsorbed with GST-AURKA (5 μg) or GST (1.8 μg) fusion proteins in a total volume of 300 μL binding buffer (20 mM HEPE, pH 7.5, 200 mM KCl, 5 mM $MgCl_2$, 0.5 mM EGTA, 1 mM dithiothreitol, 0.05% Triton X-100) for 3 h at 4 °C. The magnetic glutathione particles were then washed by 3 times with the binding buffer. The bound proteins were eluted with 5 mM glutathione/10 mM Tris (pH 8.0) and subjected to western blotting.

RNA pull-down assay
Biotinylated transcripts were transcripted from DROSHA PCR fragments with T7 promoter using MEGAscript T7 kit (Ambion, AM1333) with biotin-16-UTP (Ambion, AM8452) and then purified by RNAiso Plus (TaKaRa). Whole cell lysates (1 mg per sample) were incubated with 5 μg of purified biotinylated transcripts for 1 h at 25 °C. Complexes were isolated with Streptavidin Agarose (Invitrogen, SA10004). The co-precipitated proteins were detected by western blotting. Primers used to prepare PCR fragments were listed in Supplementary information, Table S1.

RNA-seq
Two replicate samples from MDA-MB-231 (Tet-on shAURKA) treated with or without doxycycline for 72 h were submitted to Novogene company (Beijing, China). Total RNAs were extracted according to RNeasy plus kit (Qiagen, 74104). Libraries were prepared according to the NEBNext® UltraTM RNA Library Prep Kit for Illumina® (NEB) following the manufacturer's recommendations. All samples were sequenced by illumina Hiseq platform with pair end 125 bp read length. The RNA-seq data were mapped to the reference genome hg19 using the software Hisat2 v2.0.5 based on the default parameters. DEGs were analyzed using DEseq2.[43] Genes with an adjusted *P* value < 0.05 and FC > 1.5 were assigned as differentially expressed. Data accession: all the raw data have been deposited in the GEO under GSE128428.

Microarray
Two replicate RNA samples of MDA-MB-231 shDROSHA cells and shNC cells were extracted by RNAiso Plus and submitted to the Gene Tech Company Limited (Shanghai, China) for labeling and hybridization for 16 h at 45 °C using Affymetrix Clariom D. Microarray scans were obtained with a GeneChip Scanner 3000 7 G (Affymetrix) using the default settings. Data were normalized with the Robust Multichip Analysis (RMA) algorithm using default analysis settings and some additional median/quantile normalization. We eliminated all probes with a means < 6.0 and standard deviation < 1.0 to filter the number of probes. Then, we filter the genes with a FC > 1.5 and *P* value < 0.05. Data accession: all the raw data have been deposited in the GEO under GSE125705.

IHC and scoring
The tissue microarray was obtained from OUTDO BIOTECH (HBreD030CS01, HBreD030PG04). Antigen retrieval was performed by heating the sample in EDTA buffer (pH 8.0) in a microwave oven for 15 min. The slides were stained for 25 min at room temperature (RT). Histological detection of DROSHA (ab183732, Abcam), STC1 (ab229477, Abcam) or NANOG (GTX100863, GeneTex) was performed using EnVision Detection Systems. The IHC staining was quantified as the H-score, which has been validated for breast cancer IHC staining.[44] The images were acquired using a Nuance EX multispectral imaging system (PerkinElmer) under identical conditions; two fields of each sample in the tissue microarray were acquired using a 20× objective. Scoring was performed using inForm software

(PerkinElmer). Typical images corresponding to negative (four images, scored as '0'), weak (four images, scored as '1'), intermediate (four images, scored as '2') and strong (four images, scored as '3') brown staining were selected by two independent experienced pathologist for software training. During training, an algorithm, which helps the software to distinguish between the cancer and non-cancer tissues, and distinguish between the nuclear and cytoplasmic regions, and sets the thresholds for 0–3 staining, was optimized. Next, the optimized algorithm was used to perform scoring of the other samples. The H-score (between 0 and 300) for each sample was calculated in the following way: (% of cells stained at intensity 1 × 1) þ (% of cells stained at intensity 2 × 2) þ (% of cells stained at intensity 3 × 3). The receiver operating characteristic curve analysis was used to select the cut-off point for each variable.

GSEA

The gene set enrichment analysis software (GSEA v2.1.0) was used to identify the molecular phenotype of downregulated genes in shDROSHA microarray data. The gene expression signatures were acquired from published microarray dataset.[45] Gene sets with a nominal P value < 0.05 and FC > 1.25 were considered significant hits.

Molecular dynamics (MD) simulation

The crystallographic structure of β-Catenin (PDB ID: 3TX7) was obtained from RCSB Protein Data Bank. The 3D structure of DROSHA was predicted using I-TASSER Server.[46] The conformation of the complexes formed between β-Catenin and DROSHA were predicted using Zdock program. MD simulations were performed by Gromacs 5.1.5 with Amber99sb force field. After MD simulation, the molecular mechanics energies combined with the Poisson-Boltzmann and surface area continuum solvation (MM/PBSA) methods were employed to evaluate the binding free energy of β-Catenin with DROSHA.[18] The interaction residues between these two proteins were analyzed using LIGPLOT (v.4.4.2).[47]

The crystallographic structure of AURKA (PDB ID: 5G1X) was obtained from RCSB Protein Data Bank. The 3D structure of IGF2BP3 RRM domain (amino acid: 1–157) was predicted using existing crystal structure of IGF2BP2 (PDB ID: 6FQ1) as template by Swiss Model Server.[48] The conformation of the complexes formed between AURKA and IGF2BP2 were predicted using Zdock program and all of the MD simulations were performed by Gromacs 5.1.5 with Amber99sb force field. After MD simulation, the molecular mechanics energies combined with the Poisson-Boltzmann and surface area continuum solvation (MM/PBSA) methods were employed to evaluate the binding free energy of AURKA with IGF2BP2.[18] The interaction residues between these two proteins were analyzed using LIGPLOT (v.4.4.2).[47]

$ALDH^+$ cell staining

The ALDEFLUOR assay was carried out according to the manufacturer's guidelines (STEMCELL Technologies, 01700). Briefly, cells were suspended in ALDEFLUOR assay buffer containing an ALDH substrate, BODIPY-aminoacetaldehyde (BAAA) and incubated for 30 min at 37 °C. To distinguish between $ALDH^+$ and $ALDH^-$ cells, a fraction of cells was incubated with a 10-fold excess of an ALDH inhibitor, Diethylamino-benzaldehyde. The result in fluorescence intensity of $ALDH^+$ cells was analyzed by flow cytometer (Beckman Coulter, CytoFLEX).

Sphere formation assay

For replating sphere formation, cells were seeded in 6-well ultralow attachment plates (Corning, 3471) at a density of 1×10^3 cells/well with sphere medium. After 7 days, the number and diameter of tumor spheres were calculated with the inverted microscope (Olympus, DP73). Then, cells were digested with trypsin and replanted into 6-well ultralow attachment plates at a density of 1×10^3 cells/well. After another 7 days, the number and diameter of spheres were calculated.

For Extreme limiting dilution assay (ELDA), cells were seeded into 96-well ultralow attachment plates (Corning, 3474) with sphere medium at density of 1, 5, 10, 20, 50, 100 cells/well (24 wells per cell density). After 7 days, positive (sphere formation) well numbers in each group were uploaded and calculated in the ELDA website.[49]

Sphere medium includes DMEM/F12 (Gibco, C11330500BT), 20 ng/mL basic fibroblast growth factor (Petrotech, 100-18B), 20 μL/mL B27 (Thermo Fisher Scientific, 17504044) and 20 ng/mL epidermal growth factor (Petrotech, 100-05).

Animal studies

Female BALB/c nude mice (4–6 weeks, Beijing Vital River Laboratory Animal Technology Co., Ltd) subcutaneous were injected with the indicated MDA-MB-231 cells (10^5 cells/0.1 mL/mouse). The tumor volumes were measured by a calliper once every three days and estimated using the formula $= 0.5 \times a \times b^2$ (a and b were the long and short diameter of the tumors, respectively). Mice were sacrificed after about four weeks and the xenografted tumors were immediately dissected to take photos.

For secondary limited dilution xenograft, primary xenografted tumors were digested with both collagenase I (Sigma, C0130) and hyaluronidase (Sigma, H1136). Serially diluted single cell suspensions (10^5, 10^4, 10^3, 10^2) were subcutaneously injected into nude mice (4–6 weeks old). After about four weeks, tumor formation ability was calculated using the Extreme Limiting Dilution Analysis software.[49]

All animal studies were approved by the Institute Animal Care and Use Committee (IACUC) of Dalian Medical University (No. AAE18017) and carried out in accordance with established institutional guidelines and approved protocols.

ChIP assay

ChIP Assay was conducted with ChIP-IT Express Chromatin Immunoprecipitation Kits (Active Motif). In short, fix 1×10^7 cells with fixation solution for 10 min at RT, then wash cells with ice-cold 1× PBS and rock the plate for 5 s and discard PBS. Stop fixation reaction with Glycine Stop-fix Solution and rock the plate at RT for 5 min. Scrape cells with ice-cold cell Scraping Solution including PMSF (final concentration is at 0.6 mM) and centrifuge cells at 2500 rpm for 10 min at 4 °C. Resuspend cells with 1 mL ice-cold Lysis Buffer for 30 min. Transfer cells to an ice-cold dounce homogenizer and dounce with 10 stokes to aid in nuclei release. Shear the DNA with the sonicator. Store 10 μL chromatin as "Input DNA" at −20 °C. The other chromatin was immunoprecipitated with 2 μg DROSHA antibody (3364S, CST) or corresponding rabbit IgG antibody (CST, 7074) and protein A/G magnetic beads at 4 °C overnight. Wash beads with ChIP Buffer I and ChIP Buffer II. Elute immune complex with 50 μL Elution Buffer AM2. Add 50 μL Reverse Cross-linking Buffer to elute chromatin. Incubate chromatin with 2 μL Proteinase K at 37 °C for 1 h and get DNA with phenol and phenol/chloroform extractions. The specific primers used for PCR targeting *STC1* promoter were listed in Supplementary information, Table S1.

Software

JASPAR was used to predict the potential binding of transcription factors (TFs) on the STC1 "core promoter" region, from +402 to −1810 relative to the transcription start site (TSS).[50] We identified top 100 highly expressed genes in breast tumors with the assistant of Gene Expression Profiling Interactive Analysis (GEPIA) with default setting.[51] We also identified DROSHA correlated genes in breast cancer (METABRIC dataset) with the assistant of cBioPortal.[52] The m^6A site prediction was performed by "RMBase v2.0".[53] Hazardous ratios (HRs) for tumor cohorts of breast cancer were determined by

the Kaplan–Meier (KM) plotter online tool using best cutoff analyses and the multigene classifier.[54] The overall survival (OS) of breast cancer patients were analyzed using a Kaplan–Meier survival plot.

Statistical analysis

Statistical comparisons were performed by using Student's *t*-test (two-tailed unpaired), ANOVA test or χ^2 test as indicated in the figure legends. Statistical analysis for correlation was performed using two-tailed Pearson's correlation test. Data were presented as means ± SD, $P < 0.05$ was considered significant.

DATA AVAILABILITY

The RNA-seq and microarray data generated by this study have been deposited in the GEO database under the accession number GSE128428 (RNA-seq) and GSE125705 (microarray). Human breast tumor gene expression and clinical data were derived from TCGA Research Network (http://cancergenome.nih.gov/). Previously published meRIP-seq data and microarray data were re-analyzed. They are available under accession codes: GSE60213, GSE29714, GSE90642 and GSE54365 for meRIP-seq; GSE7513 and GSE15192 for microarray.

ACKNOWLEDGEMENTS

This work was supported by the National Key R&D Program of China (2019YFA0110300 to Q.Liu and 2017YFA0505600-04 to Q.Liu), the National Natural Science Foundation of China (81820108024 to Q.Liu, 81630005 to Q.Liu, 81972786 to J.X., 81573025 to Q.Liu, 81703062 to L.H. and 81703091 to F.A.), Program for Changjiang Scholars and Innovative Research Team in University of Ministry of Education of China (IRT_17R15), Innovative Research Team in University of Liaoning (LT2017001 to Q.Liu), the Natural Science Foundation of Liaoning (2019-BS-081 to F. P.), the "Seedling cultivation" program for young scientific and technological talents of Liaoning (LZ2019067 to B.C. and 2020 to F.P.), the program for climbing Scholars of Liaoning, the Science and Technology Innovation Foundation of Dalian (2020JJ25CY008 to Q.Liu), Dalian High-level Talent Innovation Program (2016RD12 to Q.Liu), International Scientific and Technological Cooperation of Dalian (2015F11GH095 to Q.Liu), the Natural Science Foundation of Guangdong (2016A030311038 and 2017A030313608 to Q.Liu, 2017A020215098 to Z.W.), the Science and Technology Planning Project of Guangzhou (201804020044 to Q.Liu). E. W-F.L.'s work is supported by MRC (MR/N012097/1), CRUK (C37/A12011; C37/18784), Breast Cancer Now (2012MayPR070; 2012NovPhD016; 2014NovPhD326). The authors thank Prof. Yungui Yang (Beijing Institute of Genomics, CAS) for scientific advice and technical assistance, especially meRIP-seq data analysis and the method of meRIP-qPCR assay. The authors thank Prof. Lingqiang Zhang (Beijing Institute of Lifeomics, Beijing, China) for a gift of HA-Ub plasmid.

AUTHOR CONTRIBUTIONS

Q.Liu, J.X and F.P. conceived and designed the entire project. Q.Liu, F.P., J.X., B.H. and Z. W., designed and supervised the research. F.P., B.C., Q.Liang, S.Z., H.Zou, M.L., H.Zhao, Y. M., J.H. and J.Z. performed the experimental data analyses and/or experimental planning. H.Zou, Y.L., J.L. and Z.L., performed the transcriptome-wide and meRIP-seq data analyses. B.L., S.L., J.C. and F.W. performed the proteomic analyses by LC-MS. P.C. and Z.S. performed MD simulation. F.A. drafted the working model. L.X. collected breast tumor specimens and conjugated normal breast specimens. Q.Liu, J.X., F.P., B.C. and E. W-F.L. contributed reagents/analytic tools and/or grant support. F.P., B.C., Q.Liu, J.X., B.H., Q.Liang, S.Z., Y.Z. and E.W-F.L. wrote and revised the manuscript. All authors discussed the results and commented on the manuscript.

ADDITIONAL INFORMATION

Supplementary information accompanies this paper at https://doi.org/10.1038/s41422-020-00397-2.

Competing interests: The authors declare no competing interests.

REFERENCES

1. Han, J. et al. Posttranscriptional crossregulation between Drosha and DGCR8. *Cell* **136**, 75–84 (2009).
2. Melamed, Z. et al. Alternative splicing regulates biogenesis of miRNAs located across exon-intron junctions. *Mol. Cell* **50**, 869–881 (2013).
3. Nepal, C. et al. Transcriptional, post-transcriptional and chromatin-associated regulation of pri-miRNAs, pre-miRNAs and moRNAs. *Nucleic Acids Res.* **44**, 3070–3081 (2016).
4. Wagschal, A. et al. Microprocessor, Setx, Xrn2, and Rrp6 co-operate to induce premature termination of transcription by RNAPII. *Cell* **150**, 1147–1157 (2012).
5. Lin, S. & Gregory, R. I. MicroRNA biogenesis pathways in cancer. *Nat. Rev. Cancer* **15**, 321–333 (2015).
6. Hata, A. & Kashima, R. Dysregulation of microRNA biogenesis machinery in cancer. *Crit. Rev. Biochem. Mol. Biol.* **51**, 121–134 (2016).
7. Lu, W. T. et al. Drosha drives the formation of DNA:RNA hybrids around DNA break sites to facilitate DNA repair. *Nat. Commun.* **9**, 532 (2018).
8. Gromak, N. et al. Drosha regulates gene expression independently of RNA cleavage function. *Cell Rep.* **5**, 1499–1510 (2013).
9. Wang, X., Zhao, X., Gao, P. & Wu, M. c-Myc modulates microRNA processing via the transcriptional regulation of Drosha. *Sci. Rep.* **3**, 1942 (2013).
10. Zhao, B. S., Roundtree, I. A. & He, C. Post-transcriptional gene regulation by mRNA modifications. *Nat. Rev. Mol. Cell Biol.* **18**, 31–42 (2017).
11. Yang, Y., Hsu, P. J., Chen, Y. S. & Yang, Y. G. Dynamic transcriptomic m6A decoration: writers, erasers, readers and functions in RNA metabolism. *Cell Res.* **28**, 616–624 (2018).
12. Deng, X., Su, R., Feng, X., Wei, M. & Chen, J. Role of N6-methyladenosine modification in cancer. *Curr. Opin. Genet. Dev.* **48**, 1–7 (2018).
13. Zhang, S. et al. m6A demethylase ALKBH5 maintains tumorigenicity of glioblastoma stem-like cells by sustaining FOXM1 expression and cell proliferation program. *Cancer Cell* **31**, 591–606 (2017).
14. Weng, H. et al. METTL14 inhibits hematopoietic stem/progenitor differentiation and promotes leukemogenesis via mRNA m6A modification. *Cell Stem Cell* **22**, 191–205 (2018).
15. Chen, M. et al. RNA N6-methyladenosine methyltransferase-like 3 promotes liver cancer progression through YTHDF2-dependent posttranscriptional silencing of SOCS2. *Hepatology* **67**, 2254–2270 (2018).
16. Huang, H. et al. Recognition of RNA N6-methyladenosine by IGF2BP proteins enhances mRNA stability and translation. *Nat. Cell Biol.* **20**, 285–295 (2018).
17. Yan, M. et al. Aurora-A kinase: a potent oncogene and target for cancer therapy. *Med. Res. Rev.* **36**, 1036–1079 (2016).
18. Zheng, F. et al. Nuclear AURKA acquires kinase-independent transactivating function to enhance breast cancer stem cell phenotype. *Nat. Commun.* **7**, 10180 (2016).
19. Clarke, M. F. Clinical and therapeutic implications of cancer stem cells. *N. Engl. J. Med.* **380**, 2237–2245 (2019).
20. Geula, S. et al. Stem cells. m6A mRNA methylation facilitates resolution of naive pluripotency toward differentiation. *Science* **347**, 1002–1006 (2015).
21. Seita, J. et al. Gene expression commons: an open platform for absolute gene expression profiling. *PloS One* **7**, e40321 (2012).
22. Han, J. et al. The Drosha-DGCR8 complex in primary microRNA processing. *Genes Dev.* **18**, 3016–3027 (2004).
23. Bourguignon, L. Y., Spevak, C. C., Wong, G., Xia, W. & Gilad, E. Hyaluronan-CD44 interaction with protein kinase C(epsilon) promotes oncogenic signaling by the stem cell marker Nanog and the Production of microRNA-21, leading to down-regulation of the tumor suppressor protein PDCD4, anti-apoptosis, and chemotherapy resistance in breast tumor cells. *J. Biol. Chem.* **284**, 26533–26546 (2009).
24. Fustin, J. M. et al. RNA-methylation-dependent RNA processing controls the speed of the circadian clock. *Cell* **155**, 793–806 (2013).
25. Pendleton, K. E. et al. The U6 snRNA m6A methyltransferase METTL16 regulates SAM synthetase intron retention. *Cell* **169**, 824–835 (2017).
26. Li, Y. et al. Stanniocalcin-1 augments stem-like traits of glioblastoma cells through binding and activating NOTCH1. *Cancer Lett.* **416**, 66–74 (2018).
27. Cao, J. X. et al. E2F1-regulated DROSHA promotes miR-630 biosynthesis in cisplatin-exposed cancer cells. *Biochem. Biophys. Res. Commun.* **450**, 470–475 (2014).
28. Wang, X. et al. N6-methyladenosine-dependent regulation of messenger RNA stability. *Nature* **505**, 117–120 (2014).
29. Niu, Y., Wan, A., Lin, Z., Lu, X. & Wan, G. *N6*-methyladenosine modification: a novel pharmacological target for anti-cancer drug development. *Acta Pharm. Sin. B* **8**, 833–843 (2018).
30. Vu, L. P., Cheng, Y. & Kharas, M. G. The Biology of m6A RNA methylation in normal and malignant hematopoiesis. *Cancer Discov.* **9**, 25–33 (2019).
31. Tan, J. et al. Pharmacologic disruption of polycomb-repressive complex 2-mediated gene repression selectively induces apoptosis in cancer cells. *Genes Dev.* **21**, 1050–1063 (2007).
32. Mayr, C. et al. 3-deazaneplanocin A may directly target putative cancer stem cells in biliary tract cancer. *Anticancer Res.* **35**, 4697–4705 (2015).
33. Liu, J. et al. m6A mRNA methylation regulates AKT activity to promote the proliferation and tumorigenicity of endometrial cancer. *Nat. Cell Biol.* **20**, 1074–1083 (2018).

34. Du, Y. et al. SUMOylation of the m6A-RNA methyltransferase METTL3 modulates its function. *Nucleic Acids Res.* **46**, 5195–5208 (2018).
35. Zhou, J. et al. Dynamic m(6)A mRNA methylation directs translational control of heat shock response. *Nature* **526**, 591–594 (2015).
36. Shi, H., Wei, J. & He, C. Where, when, and how: context-dependent functions of RNA methylation writers, readers, and erasers. *Mol. Cell* **74**, 640–650 (2019).
37. Bertero, A. et al. The SMAD2/3 interactome reveals that TGFbeta controls m6A mRNA methylation in pluripotency. *Nature* **555**, 256–259 (2018).
38. Sanjana, N. E., Shalem, O. & Zhang, F. Improved vectors and genome-wide libraries for CRISPR screening. *Nat. Methods* **11**, 783–784 (2014).
39. Cui, B. et al. Stress-induced epinephrine enhances lactate dehydrogenase A and promotes breast cancer stem-like cells. *J. Clin. Invest.* **129**, 1030–1046 (2019).
40. Dominissini, D., Moshitch-Moshkovitz, S., Salmon-Divon, M., Amariglio, N. & Rechavi, G. Transcriptome-wide mapping of N(6)-methyladenosine by m(6)A-seq based on immunocapturing and massively parallel sequencing. *Nat. Protoc.* **8**, 176–189 (2013).
41. Meyer, K. D. et al. Comprehensive analysis of mRNA methylation reveals enrichment in 3' UTRs and near stop codons. *Cell* **149**, 1635–1646 (2012).
42. Shevchenko, A., Tomas, H., Havlis, J., Olsen, J. V. & Mann, M. In-gel digestion for mass spectrometric characterization of proteins and proteomes. *Nat. Protoc.* **1**, 2856–2860 (2006).
43. Love, M. I., Huber, W. & Anders, S. Moderated estimation of fold change and dispersion for RNA-seq data with DESeq2. *Genome Biol.* **15**, 550 (2014).
44. Detre, S., Saclani Jotti, G. & Dowsett, M. A "quickscore" method for immunohistochemical semiquantitation: validation for oestrogen receptor in breast carcinomas. *J. Clin. Pathol.* **48**, 876–878 (1995).
45. Creighton, C. J. et al. Residual breast cancers after conventional therapy display mesenchymal as well as tumor-initiating features. *Proc. Natl. Acad. Sci. USA* **106**, 13820–13825 (2009).
46. Yang, J. et al. The I-TASSER Suite: protein structure and function prediction. *Nat. Methods* **12**, 7–8 (2015).
47. Feng, L. et al. De novo molecular design of a novel octapeptide that inhibits in vivo melanogenesis and has great transdermal ability. *J. Med. Chem.* **61**, 6846–6857 (2018).
48. Waterhouse, A. et al. SWISS-MODEL: homology modelling of protein structures and complexes. *Nucleic Acids Res.* **46**, W296–W303 (2018).
49. Hu, Y. & Smyth, G. K. ELDA: extreme limiting dilution analysis for comparing depleted and enriched populations in stem cell and other assays. *J. Immunol. Methods* **347**, 70–78 (2009).
50. Mathelier, A. et al. JASPAR 2014: an extensively expanded and updated open-access database of transcription factor binding profiles. *Nucleic Acids Res.* **42**, D142–D147 (2014).
51. Tang, Z. et al. GEPIA: a web server for cancer and normal gene expression profiling and interactive analyses. *Nucleic Acids Res.* **45**, W98–W102 (2017).
52. Gao, J. et al. Integrative analysis of complex cancer genomics and clinical profiles using the cBioPortal. *Sci. Signal.* **6**, pl1 (2013).
53. Xuan, J. J. et al. RMBase v2.0: deciphering the map of RNA modifications from epitranscriptome sequencing data. *Nucleic Acids Res*. **46**, D327–D334 (2018).
54. Lanczky, A. et al. miRpower: a web-tool to validate survival-associated miRNAs utilizing expression data from 2178 breast cancer patients. *Breast Cancer Res. Treat.* **160**, 439–446 (2016).